

RESEARCH

Open Access



# Identifying TNFSF4<sup>low</sup>-MSCs superiorly treating idiopathic pulmonary fibrosis through Tregs differentiation modulation

Yuanyuan Xie<sup>1†</sup>, Qing Yi<sup>2†</sup>, Congwang Xu<sup>3†</sup>, Yaping Wang<sup>3</sup>, Yue Jiang<sup>1</sup>, Yirui Feng<sup>4</sup>, Liudi Wang<sup>1</sup>, Hui Yang<sup>1</sup>, Yingwei Zhang<sup>5\*</sup> and Bin Wang<sup>3,1,6\*</sup> 

## Abstract

**Background** Idiopathic pulmonary fibrosis is a progressive lung disorder, presenting clinically with symptoms such as shortness of breath and hypoxemia. Despite its severe prognosis and limited treatment options, the pathogenesis of idiopathic pulmonary fibrosis remains poorly understood. This study aims to investigate the therapeutic potential of mesenchymal stromal cells in treating idiopathic pulmonary fibrosis, focusing on their ability to modulate regulatory T cells through the low tumor necrosis factor superfamily member 4 (TNFSF4) pathway. The goal is to identify mesenchymal stromal cells subtypes with optimal immunomodulatory effects to enhance regulatory T cells functions and ameliorate fibrosis.

**Methods** We identified the immune characteristics of idiopathic pulmonary fibrosis by mining and analyzing multiple public datasets and detecting regulatory T cells in the blood and lung tissues of idiopathic pulmonary fibrosis patients. An extensive examination followed, including assessing the impact of mesenchymal stromal cells on regulatory T cells proportions in peripheral blood and lung tissue, and exploring the specific role of TNFSF4 expression in regulatory T cells modulation. Whole-genome sequencing and cluster analysis were used to identify mesenchymal stromal cells subtypes with low TNFSF4 expression.

**Results** Mesenchymal stromal cells characterized by TNFSF4 expression (TNFSF4<sup>low</sup>-MSCs) demonstrated enhanced ability to regulate regulatory T cells subpopulations and exhibited pronounced anti-fibrotic effects in the bleomycin-induced idiopathic pulmonary fibrosis mouse model. These mesenchymal stromal cells increased regulatory T cells proportions, reduced lung fibrosis, and improved survival rates. TNFSF4–tumor necrosis factor receptor superfamily member 4 (TNFRSF4) signaling was identified as a critical pathway influencing regulatory T cells generation and function.

<sup>†</sup>Yuanyuan Xie, Qing Yi and Congwang Xu contributed equally to this work.

\*Correspondence:

Yingwei Zhang  
yingwei16@aliyun.com  
Bin Wang  
wangbin022800@126.com

Full list of author information is available at the end of the article



© The Author(s) 2025. **Open Access** This article is licensed under a Creative Commons Attribution-NonCommercial-NoDerivatives 4.0 International License, which permits any non-commercial use, sharing, distribution and reproduction in any medium or format, as long as you give appropriate credit to the original author(s) and the source, provide a link to the Creative Commons licence, and indicate if you modified the licensed material. You do not have permission under this licence to share adapted material derived from this article or parts of it. The images or other third party material in this article are included in the article's Creative Commons licence, unless indicated otherwise in a credit line to the material. If material is not included in the article's Creative Commons licence and your intended use is not permitted by statutory regulation or exceeds the permitted use, you will need to obtain permission directly from the copyright holder. To view a copy of this licence, visit <http://creativecommons.org/licenses/by-nc-nd/4.0/>.

**Conclusions** Our findings underscore the pivotal role of TNFSF4 in mesenchymal stromal cells mediated regulatory T cells modulation and highlight the therapeutic potential of selecting mesenchymal stromal cells subtypes based on their TNFSF4 expression for treating idiopathic pulmonary fibrosis. This approach may offer a novel avenue for the development of targeted therapies aimed at modulating immune responses and ameliorating fibrosis in idiopathic pulmonary fibrosis.

**Trial registration** Our study involved collecting 10 mL of peripheral blood from idiopathic pulmonary fibrosis patients, and the Medical Ethics Committee of Nanjing Drum Tower Hospital approved our study protocol with the approval number 2023-675-01.

**Keywords** Mesenchymal stromal cells, Regulatory T cells, TNFSF4, Idiopathic pulmonary fibrosis, Immunomodulation, Fibrosis therapy

## Background

Idiopathic pulmonary fibrosis (IPF) represents a persistent, advancing condition of the lungs marked by the transformation and scarring of fibrous tissues, which is clinically manifested by shortness of breath, hypoxemia, prominent pulmonary infiltrates on radiography, and the persistent accumulation of fixed fibrosis [1, 2]. The pathogenesis of IPF is complex and unclear. Environmental, genetic and other unknown factors lead to fibroblast-to-myofibroblast transformation, damage to alveolar epithelial cells accompanied by interstitial inflammation, an increase in fibroblast numbers, an abnormal accumulation of collagen within the extracellular matrix and subsequent functional decline [3]. Individuals diagnosed with IPF have a dismal prognosis with a median survival of 5~6 years from the symptom onset and 2~4 years after diagnosis [2, 3]. Lung transplantation is currently the only curative treatment available for people with IPF, but it is not a realistic option for the majority of patients [4]. Innovative treatments such as stromal cell-based therapy are required to manage this complex progressive disease.

Mesenchymal stromal cells (MSCs) possess pluripotency, enabling them to differentiate into diverse cellular lineages, and their immunomodulatory, migratory, and low-immunogenic properties make them a promising option for treating a wide range of diseases [5, 6]. MSCs are particularly suited for treating complex diseases such as IPF due to their strong immunomodulatory and anti-inflammatory properties [7]. MSCs can influence various subsets of adaptive immune cells, such as T lymphocytes, regulatory T cells (Tregs), T-helper cells (Th), B lymphocytes, and regulatory B cells through cell-to-cell interactions and secretion of bioactive substances [8]. According to multiple studies, it has been shown that MSCs could play a therapeutic role in the bleomycin (BLM)-induced IPF model. Intravenous injection of MSCs can ameliorate the BLM-induced lung fibrosis by contributing to tissue repair through balancing the immune microenvironment, reducing inflammation, reducing fibrosis and extracellular matrix collagen deposition [9, 10]. MSCs

intervention can reduce the ability of induced antigen-specific T cell immune response in IPF models, promote the generation of Tregs and cytokines (IL-10), thus alleviating lung injury [11]. MSCs can maintain mitochondrial homeostasis in damaged lung epithelial cells of IPF mice by transferring their own mitochondria, thereby promoting tissue repair and reducing collagen deposition [12, 13]. However, in the whole MSCs-based therapy for IPF still confronted many challenges and satisfactory treatment results have not been achieved. Firstly, MSCs can originate from various tissues in the human body. Although they have universal characteristics of MSCs, the heterogeneity of MSCs, attributed to tissue origin and donor variability, may influence their therapeutic effects in fibrotic diseases, potentially related to variations in their immunomodulatory capacity. Numerous comparative studies on MSCs heterogeneity have suggested that MSCs from different sources may have varying clinical therapeutic effects on specific diseases [14–16]. In our former study, treatment with umbilical cord-derived MSCs (UCMSCs) from different donor sources in a mouse model of liver fibrosis revealed that UCMSCs with a highly promoting Tregs differentiation phenotype were the optimal effective in treatment [17]. To our knowledge, there are not enough animal models or clinic trials to investigate the differential efficacies of MSCs from different sources to screen out optimal cell types for IPF treatment. Secondly, many current MSCs-based therapies for IPF are based on the universal biological functions of MSCs, such as factor secretion and/or immune regulation capability, and lack the specific target molecule or signaling of the main etiology or pathogenesis of diseases to elucidate the therapeutic mechanism. In addition, MSCs used in many experiments were isolated and expanded in common laboratory condition, and had not undergone strict quality control and testing. Some MSCs also were contaminated with imperceptible micro-organism such as Chlamydia and Mycoplasma in ordinary environments, and their biological activities were altered, resulting in incomparable results among different researches.

We first included multiple public peripheral blood (PB) mononuclear cells (PBMCs) datasets of IPF patients and healthy individuals from the Gene Expression Omnibus (GEO). By merging samples, we analyzed the immune cell characteristics and functions of Tregs in IPF patients using both array and sequencing data. Through the collection and testing of clinical patient samples, we found that there was a remarked decrease in peripheral Tregs in blood and lung tissue in IPF patients compared with healthy people, consistent with previous studies [18, 19]. Tregs are a class of cells that play an essential role in maintaining immune homeostasis and peripheral tolerance, and the deletion of Tregs leads to lethal autoimmune diseases in humans and mice [20]. The proportion and function of Tregs have been found to be relevant to a variety of fibrosis progression. Reduced proportions of Tregs have been observed in biliary atresia-associated liver fibrosis and pulmonary fibrosis [18, 21]. MSCs can interact with macrophages, recruit Tregs, and suppress inflammatory T cell subsets, thereby attenuating lung fibrosis [22, 23]. Transplantation of MSCs has been shown to increase Tregs proportions and alleviate fibrosis, thereby prolonging survival [24, 25]. Whether Tregs play the role of friend or foe in IPF depends on IPF progression stage. Previous reports have proven that the CXCL12/CXCR4 axis is crucial in IPF, with CXCR4<sup>+</sup> fibroblasts being recruited to the lungs of IPF patients, while Tregs have been found to reduce the expression of CXCL12, thus potentially playing a key role in reducing the recruitment of fibroblasts [26]. Furthermore, Tregs have also been found to inhibit the recruitment of fibroblasts by suppressing FGF-9 and can prevent fibrosis induced by TGF- $\beta$ 1 through the release of IL-10 [27, 28]. Therefore, in this study we designed a new strategy of MSCs-based therapy for IPF. We screened out optimal subset of MSCs aiming to the main pathogenesis of IPF from clinic-grade MSCs derived from multiple tissue sources, and investigated their therapeutic efficacies to elucidate the definite therapeutic mechanism, providing reliable evidences for clinical application.

In compliance with current Good Manufacturing Practice (cGMP) standards, as outlined in our prior research, we produced clinical-grade MSCs from a variety of sources including healthy human bone marrow (BM), UC, adipose tissue (AD), dental pulp (DP), gingival tissue, placental villi, amnion, and meconium, all within sterile conditions [29]. These MSCs were subject to thorough safety, quality, and efficacy assessments, meeting not just the foundational criteria for biological products but also adhering to cell therapy regulations and contemporary testing methodologies, setting quality benchmarks for MSC-based clinical treatments [30, 31]. Then we found subtype of MSCs characterized by low tumor necrosis factor superfamily member 4 (TNFSF4) expression

demonstrated a marked capability to regulate Tregs subpopulations and pronounced anti-fibrotic effects of IPF. Our research highlights the significance of MSCs subpopulation in Tregs regulation and the novel pivotal role of TNFSF4 in this process, offering new insights into the therapeutic potential of MSCs in treating IPF.

## Materials and methods

### The work has been reported in line with the ARRIVE guidelines 2.0. Profiling and analysis of mRNA expression data

To explore the function of the Tregs and marker genes, multiple public datasets of PBMCs from GEO were included. Three array datasets sharing the same platform, GSE28221, GSE33566 and GSE15197 were integrated, to increase the reliability of the data by merging the sample, and finally obtained 186 cases and 62 controls. Another sequencing dataset GSE134692 was analyzed alone. The ComBat method was used to adjust for batch effects among different datasets using the R package sva. Immune cell signatures and infiltration features were analyzed via databases [32, 33], employing ssGSEA in GSVA (version 1.44.5) to quantify T cell signature levels per sample. The differentially expressed genes (DEGs) were analyzed by function in the Limma and DESeq2 R package, separately for array and sequencing data.

### Clinical information

Patients with hospitalized IPF [ $n=21$ , 16 males and 5 females, mean age =  $(53.8 \pm 10.3)$  years] were enrolled from Nanjing Drum Tower Hospital (China). Inclusion criteria for patient: (1) The American Thoracic Society, the European Respiratory Society, the Japanese Respiratory Society, and the Latin American Thoracic Society all published diagnostic criteria for IPF patients in 2011, (2) IPF patients had not received any prior treatment before completing the examination. Exclusion criteria for patients: Patients with other known causes of interstitial lung disease (e.g., exposure to harmful environments, connective tissue diseases, drug-induced interstitial changes) were excluded. Healthy controls [ $n=23$ , 15 males and 8 females, mean age =  $(50.8 \pm 8.9)$  years] were enrolled from the Health Examination Center of the Nanjing Drum Tower Hospital. Every participant was required to submit written informed consent, and the Medical Ethics Committees of Nanjing Drum Tower Hospital approved our project titled "TNFSF4<sup>low</sup>-MSCs Improve IPF by Regulating Tregs Subtypes" clinical research protocol with the number 2023-675-01, with an approval date of March 20, 2023. Approximately 10 mL of PB was collected from each participant. The PB samples were centrifuged at 3,000 rpm for 10 min using a cryogenic high-speed frozen centrifuge (Eppendorf, Germany). This centrifugation step separated the

upper serum layer for subsequent enzyme-linked immunosorbent assay (ELISA). The ration of T cell subtypes was assessed by flow cytometry (FCM) and the relative mRNA level was determined by real-time quantitative polymerase chain reaction (qPCR).

#### ELISA

ELISA detection was used for LN-5 (MyBioSource, USA) and HAase (Sangon Biotech, China) determination in human PB. All the procedures were performed according to the manufacturer's instructions.

#### RNA isolation and qPCR

RNA was isolated from MSCs and PBMCs employing the RNA easy isolation solution provided by Vazyme (China). The quantity of the extracted RNA was determined, and a total of 1 µg of RNA was converted into cDNA using the Hiscript III reverse transcriptase from Vazyme. The composition of the qPCR mix included 2 µL of cDNA, 1 µL of gene-specific forward and reverse primers, 10 µL of SYBR Green I qPCR Master Mix, and 6 µL of ddH<sub>2</sub>O, culminating in a 20 µL reaction volume. Primer sequences, crafted by Genscript Biotechnology Corporation in Nanjing, China, are detailed in Table S1.

#### BLM-IPF model and MSCs transplantation

Animal studies were conducted strictly in accordance with the protocols and standards set by the Institutional Animal Care and Use Committee (IACUC) of Nanjing Drum Tower Hospital (DWSY-22047178). The animal protocol is titled "Research on the Mechanism of MSCs in Treating Pulmonary Fibrosis," with an approval date of April 7, 2022. Furthermore, the care and handling of laboratory animals were in strict compliance with the National Institutes of Health's Guide for the Care and Use of Laboratory Animals, as outlined in NIH publication No. 8023, revised most recently in 1978. A total of 80 mice, equally divided between females and males, were used in this study. C57BL/6J mice aged 6 to 8 weeks were anesthetized using 1% isoflurane (RWD, R510-22-10, China). Pulmonary fibrosis was induced by administering 5 mg/kg of BLM dissolved in phosphate-buffered saline (PBS) via non-invasive (using catheter). The mice with receiving BLM tracheal injection were arbitrarily assigned into different treatment groups. A total of  $5 \times 10^5$  MSCs in 300 µL PBS were intravenously injected into the tail vein of each mouse at 7 and 14 days after BLM injection. For the control group, 300 µL PBS was intravenously injected into the tail vein. The tissue samples were collected 21 days after BLM injection. The mice were placed in an automated CO<sub>2</sub> euthanasia chamber (YUYAN INSTRUMENTS, China), with a CO<sub>2</sub> flow rate set at 2 L/min. The euthanasia process lasted for 3–5 minutes, until the mice were fully euthanized,

after which tissue collection was performed including the lungs, blood, lymph nodes, and spleen. The schematic diagrams of the treatment in the mouse IPF model were shown in Fig. 1a and m.

#### Tregs depletion

For the purpose of Tregs depletion, mice received two intraperitoneal injections containing 30 µg of anti-mouse CD25 antibody (clone PC61 from BioLegend, USA) dissolved in 200 µL of PBS, administered on days 9, 13, and 17 following BLM OA exposure. Conversely, the control group was administered a solution of rat isotype IgG1 (BioLegend, USA).

#### Hydroxyproline assay and collagen measurements

To assess lung fibrosis biochemically, the hydroxyproline levels in the left lungs of mice were analyzed. The lung sections were weighed, homogenized, and then subjected to incubation in 6 M HCl at 110 °C ranging from 2 to 6 h. Post-hydrolysis, the sample's pH was neutralized to a neutral range of 6–8 using NaOH. The concentration of hydroxyproline in these samples was ascertained by recording the absorbance at 560 nm using a microplate reader from Molecular Devices, and the results were calibrated against standard curves provided by Solarbio, China. Additionally, the collagen content was quantified utilizing the Sircol® soluble collagen assay from Biocolor, UK, with right lung biopsies being employed for the analysis.

#### Immunohistochemical staining

Lung tissues from healthy individuals and IPF patients, procured from Nanjing Drum Tower Hospital's Pathology Department, underwent immunohistochemical staining on paraffin sections to evaluate Tregs infiltration, specifically detecting Foxp3<sup>+</sup> cells using a kit (Absin, China), with nuclear staining via 4',6-diamidino-2-phenylindole (DAPI).

Experimental mice's lungs were dissected, PBS washed, fixed in 4% paraformaldehyde, paraffin-embedded, dewaxed, and sectioned at 10 µm for staining. Sections were heated (65~80 °C), processed through xylene and graded alcohols, then water rinsed. Endogenous peroxidase was quenched with 3% hydrogen peroxide, followed by antigen retrieval in diluted solution and blocking with 5% serum. Primary antibodies (α-SMA, diluted 1:200; ColI, diluted 1:5000) were incubated overnight at 4 °C, followed by incubation of the secondary antibody at room temperature for 2 h. Tissue sections were stained with hematoxylin, developed with diaminobenzidine, dehydrated in alcohols, cleared in xylene, and sealed with neutral resin for microscopic analysis.



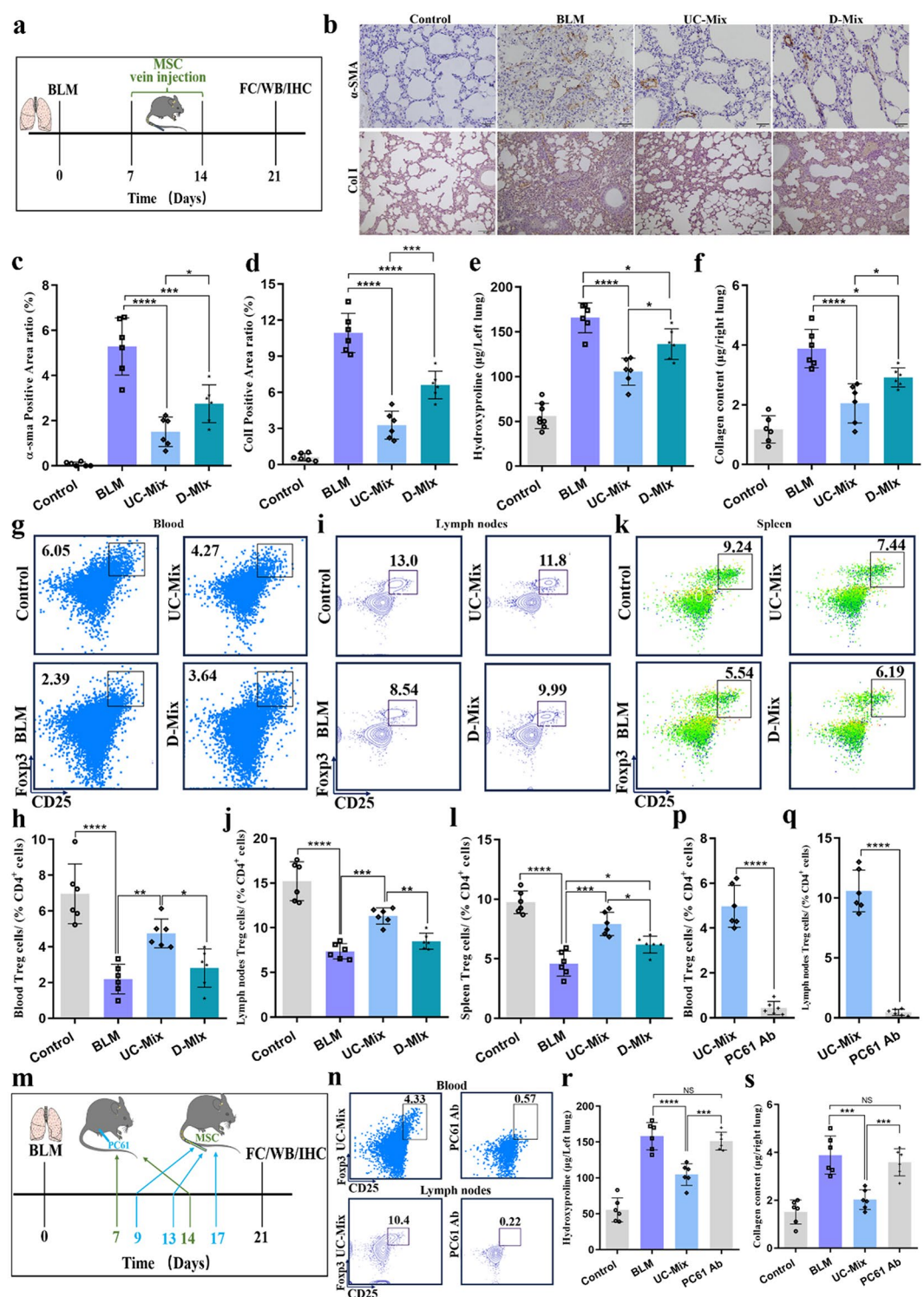


**Fig. 1** (See legend on next page.)

**Isolation and expansion of clinic-grade MSCs derived from eight tissues**

All samples used for MSCs isolation in this study were obtained from donors at Nanjing Drum Tower Hospital. Prior to participation, informed consent was obtained

from each subject with the approval of the Institutional Review Board (Project title: Utilization of Clinical Patient Samples (Tissue/Blood/Body Fluids) and Aborted Fetal Tissue to Extract Stromal Cells for Basic and Clinical Research in Regenerative Medicine and Treatment of

(See figure on previous page.)

**Fig. 1** UCMSCs with stronger Tregs-regulatory capacities have superior IPF therapeutic effects compared to DMSCs. **(a)** Flowchart of UCMSCs/DMSCs treatment of BLM-induced IPF mice. **(b–d)** Representative immunohistochemistry images for  $\alpha$ -SMA, Col I and quantification; scale bar, 20  $\mu$ m. **(e)** The-Hydroxyproline levels in the lungs. **(f)** The Collagen content in the lungs using Sircol® soluble collagen assay kit. **(g–h)** The Tregs ( $CD4^+CD25^+Foxp3^+$ ) levels in the blood of BLM-induced IPF mice treated with UC-Mix and D-Mix, determined by FCM. **(i–j)** The Tregs ( $CD4^+CD25^+Foxp3^+$ ) levels in the thoracic lymph nodes of BLM-induced IPF mice treated with UC-Mix and D-Mix, determined by FCM. **(k–l)** The Tregs ( $CD4^+CD25^+Foxp3^+$ ) levels in the spleen of BLM-induced IPF mice treated with UC-Mix and D-Mix, determined by FCM. **(m)** Flowchart of PC61 antibody administration in BLM-induced IPF mice-treated with UC-Mix. PC61 mAb (anti-murine CD25 ratIgG1) was used to deplete Tregs. **(n–q)** The levels of Tregs in the blood and lymph nodes of mice after blockade with the PC61 antibody, as determined by FCM. **(r–s)** The effect of PC61 antibody blockade on the efficacy of UC-Mix treatment in IPF mice via lung hydroxyproline and collagen levels. (UC-Mix/D-Mix: Clinical-grade UCMSCs/DMSCs derived from three donors were mixed in a 1:1:1 ratio to eliminate individual variations.) 3

Clinical Diseases; Approval No. 2017-161-08; Date of approval: 2017-11-30).

BM aspirates were collected from patients undergoing orthopedic surgery. Mononuclear cells were isolated through density gradient centrifugation. The specific method for isolating BM-derived MSCs (BMMSCs) was referenced from a previous report [34]. Fresh UC segments, approximately 15 cm in length, were obtained from full-term infants to obtain primary UCMSCs using tissue grafting methods [35]. Human adipose tissue samples were acquired from elective plastic surgery procedures. DP samples were obtained from normally exfoliated deciduous incisors of children aged 7 to 8 years. Gingival tissue samples were obtained from healthy adult patients who underwent orthodontic surgery. Chorion, amnion, and meconium samples were collected from the same healthy full-term placenta. Digestive enzyme culture methods were employed to isolate primary AD-derived MSCs (ADMSCs), DP-derived MSCs (DPMSCs), gingival-derived MSCs (GMSCs), placental villous MSCs (PCMSCs), amniotic MSCs (AMSCs), and decidua MSCs (DMSCs), as reported in previous studies [36–39]. Detailed experimental methods and regulators can be found in our previous paper [29]. The MSCs obtained were manufactured in GMP cell centers following strict Standard Operating Procedures and underwent thorough quality control to ensure compliance with clinic-grade MSC criteria [29].

**RNA isolation, library preparation, and sequencing analysis** OE Biotech Co., Ltd. (Shanghai, China) oversaw RNA extraction, library creation, and transcriptome analysis. For RNA-seq data, gene read counts were determined, calculating Transcripts Per Million (TPM); genes with  $TPM < 1$  across samples or mean  $TPM < 0.5$  were removed, with expression values log-transformed. Using *seurat*, t-SNE plotted gene expression data in two dimensions, clustering similar expression patterns. GSVA was used to calculate immune score as described above. Differential gene set enrichment across tissues used ANOVA and Tukey's test. DESeq2 identified DEGs between UCMSCs and DPMSCs, applying the false discovery rate (FDR) method for significance ( $P < 0.05$ ), with  $|\log_2$  fold

change|  $> 1$  criteria. KEGG pathway analysis elucidated the biological functions of these DEGs [40].

### Cell culture

MSCs were cultured in Dulbecco's Modified Eagle Medium (DMEM) (Gibco, USA) with the addition of 10% MSCs-qualified fetal bovine serum (FBS) (Gibco, USA) at 37 °C in an incubator with 5% CO<sub>2</sub>. In our studies, to eliminate individual variations, clinic-grade UCMSCs derived from three donors (UC-1, UC-2, UC-3) were mixed in a 1:1:1 ratio for subsequent experiments named as UC-Mix. Similarly, clinic-grade DMSCs derived from three donors (D-1, D-2, D-3) were mixed at 1:1:1 ratio named as D-Mix. All MSCs used in the study were within passages 4 to 8 to avoid the cellular senescence.

Human fetal lung fibroblasts (Helf) were cultured and then diluted in DMEM supplemented with 10% FBS, 100 IU/ mL penicillin, and 100 mg/ mL streptomycin before being used for culture and dilution.

### Quality examination of MSCs

All types of MSCs undertook the systematic quality examination and met the general quality requirements for MSC clinic therapy. The detailed experimental reagents and methods for surface marker expression, multilineage differentiation and immune modulation function test of MSCs could be referred to our previous research [29].

### FCM

Lymphocytes were extracted from human PB and diverse mouse lymphoid tissues, stained with fluorescence-tagged antibodies acquired from BD Biosciences and Thermo Fisher Scientific at room temperature for 30 min. These antibodies include BD Biosciences' CD3-PERCP (SK7), CD8-APC (SK1), IFN- $\gamma$ -FITC (25723.11), IL17 $\alpha$ -PE (N49-653), CD38-BV605 (HB7), HLA-DR-PE-cy7 (G46-6), CD45RA-PE-cy7 (HI100), CCR7-BV421 (150503), Ki67-BV421 (B56), and from Thermo Fisher Scientific, CD4-FITC (RPA-T4, GK1.5), CD25-APC (CD25-4E3, PC61.5), and Foxp3-PE (236 A/E7, FJK-16s). For the detection of intracellular cytokines, lymphocytes underwent a 4-hour stimulation using a cell activation mixture with 50 ng/ml phorbol 12-myristate 13-acetate (PMA) and 1 mM ionomycin, in the presence of brefeldin

A. The stained specimens were examined using an FACSAria™ III flow cytometer (BD Biosciences, USA) with FACSDiva software. A kit from BD Biosciences, adhering to the supplier's instructions, facilitated the intracellular cytokine staining. FCM analysis quantified the proportions of Tregs (CD4<sup>+</sup>CD25<sup>+</sup>Foxp3<sup>+</sup>), Th1 cells (CD4<sup>+</sup>IFN-γ<sup>+</sup>), and Th17 cells (CD4<sup>+</sup>IL-17A<sup>+</sup>).

#### **In vitro Tregs activation, subtyping, and proliferation assay**

Human PBMCs were separated and enriched for CD4<sup>+</sup> T cells using CD4 microbeads from Miltenyi Biotec, Germany. These CD4<sup>+</sup> T cells underwent expansion and were subsequently incubated with various MSCs. To induce Tregs differentiation, IL-2 was incorporated into the medium at a concentration of 50 U/ml. After a period of 72 h, cells in single-cell suspension were harvested for analyses focused on Tregs activation, utilizing a mix of antibodies: CD38-BV605 (HB7), HLA-DR-PE-cy7 (G46-6), CD4-FITC (RPA-T4), and CD25-APC (CD25-4E3). Further, Tregs subtyping was conducted using a set of antibodies: CD45RA-PE-cy7 (HI100), CCR7-BV421 (150503), CD4-FITC (RPA-T4), and CD25-APC (CD25-4E3), alongside Tregs proliferation assessment with Ki67-BV421 (B56), CD4-FITC (RPA-T4), CD25-APC (CD25-4E3), and Foxp3-PE (236 A/E7). Analysis of the stained cells was performed on a BD Aria III system, with data interpretation via FlowJo software.

#### **Cytometric beads assay (CBA) to detect the cytokines in intracellular**

Cytokine concentration (IL-6 and IL-10) was measured using a CBA kit (BD, USA) following the manufacturer's protocol. Subsequently, the intensity of these cells was measured with a flow cytometer. The data was analyzed using graphical user interface software FCAP Array.

#### **Immunoblotting analysis**

Total proteins were extracted using a radioimmunoprecipitation assay buffer with added protease and phosphatase inhibitors, then heated in 5 × SDS loading buffer (Beyotime, China) at 100 °C for 10 min. Subsequently, 15 µg of protein from each specimen was subjected to SDS-PAGE, followed by transfer onto PVDF membranes activated with methanol. These membranes were then incubated with 5% skim milk at ambient temperature for one hour before being exposed to primary antibodies targeting GAPDH, α-SMA, Foxp3 (Cell signalling technology, USA), collagen-1α (Thermo Fisher Scientific, USA), TNFSF4, Helios, and GTIR (Abcam, UK) overnight at 4 °C. After washing with PBST, they were treated with secondary antibodies for an hour at room temperature and visualized using enhanced chemiluminescence on a Vazyme (China) imaging system.

#### **Lentiviral ShRNA vectors transfection**

Lentiviral vectors containing *TNFSF4*-shRNA-LV3 (pGLV-h1-GFP-puro) for knockdown and *TNFSF4*-LV8 (EF-1a/mCherry&Puro) for overexpression were synthesized by Genescript (Shanghai, China). The virus titer of *TNFSF4*-shRNA-LV3 (or *TNFSF4*-LV8) was  $9 \times 10^8$  TU/ mL. In addition, a *TNFSF4*-LV8 lentivirus with red fluorescent protein (RFP) tag was constructed to verify successful transfection and overexpression. To achieve knockdown or overexpression of *TNFSF4* in MSCs, viral transfection was performed when MSCs reached 60~70% confluence, using a multiplicity of infection (MOI) of 50, as determined by pre-test results and following the manufacturer's protocol. Fluorescence microscopy was used to observe MSCs expressing green fluorescent protein (GFP) or RFP at 48 h post-transfection. Harvesting of MSCs for *TNFSF4* interference efficiency analysis was conducted at 72~96 h post-transfection. Puromycin selection (1~2 µg/mL) was initiated at 72 h post-transfection to screen and obtain stable transfected cells. The transfected cells were passaged and lyophilized for subsequent experiments.

#### **Induction of the FMT cell model**

HELf cells were plated in 6-well dishes at a concentration of  $1 \times 10^6$  cells/mL. Upon achieving the necessary confluence, the initial growth medium was removed, and the cells underwent overnight starvation in a serum-free medium for synchronization. Following adhesion, the cells were treated with TGF-β1 at a final concentration of 10 ng/mL to induce stimulation for a duration of 24 h. The supernatants from PBMCs co-cultured with different MSCs (including UC-Mix-LV, UC-Mix-TNFSF4, D-Mix-sh-LV, and D-Mix-sh-TNFSF4) for 5 days were added to the TGF-β1-stimulated Helf cells for conditional stimulation culture for 72 h. Total protein was extracted from each group of Helf cells, and the protein expression levels of α-SMA and collagen-1α were determined by Western blot analysis.

#### **In vitro blockade experiment of TNFSF4-TNFRSF4**

Within a rigorously established co-culture paradigm comprising PBMCs and DMSCs (for detailed experimental protocol, please refer to our previously published article [29]), targeted interventions were introduced through the administration of Oxelumab (anti-TNFSF4, 10 µg/mL), Amlitelimab (anti-TNFSF4, 150 µg/mL), or Telazolimab (TNFRSF4, 10 µg/mL, a monoclonal antibody that targets TNFRSF4), aiming to obstruct the TNFSF4-TNFRSF4 signaling axis. Subsequent to a cultivation period extending to the sixth day, flow cytometric analysis was conducted on the harvested PBMCs, focusing on quantifying alterations in the proportionality of Tregs relative to CD4<sup>+</sup> T lymphocytes.



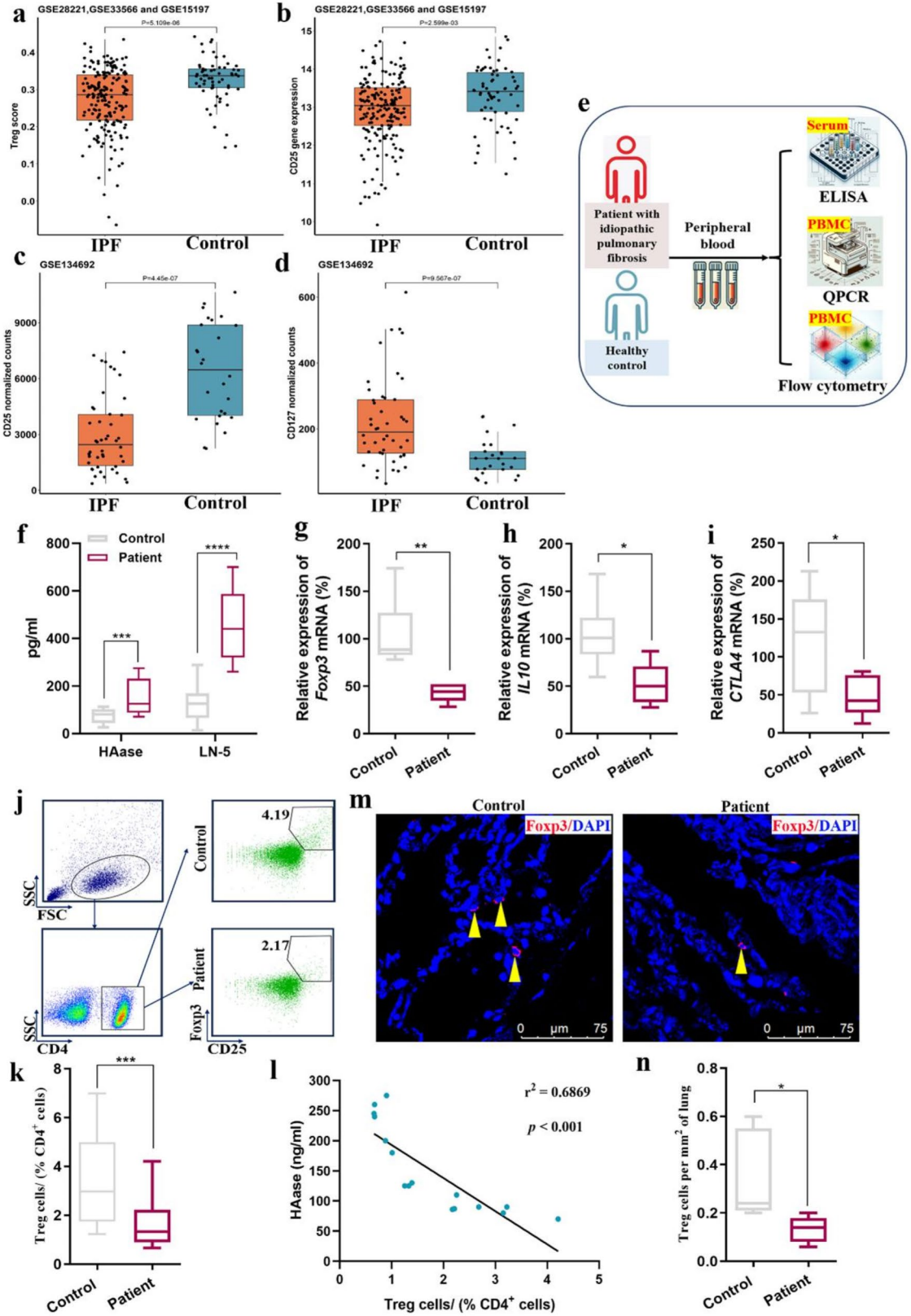


**Fig. 2** (See legend on next page.)



(See figure on previous page.)

**Fig. 2** Tregs in PB and lung tissue were significantly lower than IPF patients. **(a)** We evaluated immune infiltration using gene expression profiles from the GSE28221, GSE33566, and GSE15197 datasets from the GEO database, which include IPF samples and healthy controls. The results showed a significant decrease in Tregs scores in IPF compared to healthy controls. **(b-c)** The expression of the CD25/IL2RA gene was significantly decreased in IPF compared to healthy controls in both array and sequencing data. **(d)** The Tregs-associated negative marker gene CD127 showed a significant increase in IPF patients in the sequencing data. **(e)** PB was collected from healthy individuals and patients with IPF. The fibrosis-related proteins in serum were analyzed by ELISA. The expression of relevant genes in PBMCs was analyzed using qPCR. Additionally, CD4<sup>+</sup> T cells in PBMCs was analyzed using FCM. **(f)** The protein expression levels of HAase and LN-5 in PB were analyzed by ELISA. **(g-i)** QPCR was used to analyze the relevant gene expression of the Tregs, including IL-10, Foxp3 and CTLA4. **(j-k)** Flow cytometric analysis was performed on PBMCs to determine the percentages of Tregs (CD4<sup>+</sup> CD25<sup>+</sup> Foxp3<sup>+</sup>). Contour plots showing the cell populations from the indicated gates. **(l)** Correlation analysis between the expression of HAase and the proportions of Tregs. **(m-n)** By using immunofluorescence to stain human lung tissue paraffin sections with Foxp3 and DAPI, Tregs number in the lung tissues of healthy individuals and IPF patients was counted, followed by statistical analysis between the two groups

### Statistical analyses

Statistical evaluations were performed with GraphPad Prism 9.0 software (GraphPad Software Inc.). Normal distribution led to the use of parametric methods; in their absence, nonparametric methodologies like the Mann-Whitney tests, supplemented by Dunn's post hoc analysis, were employed. For data meeting the homogeneity of variance criterion, the analysis proceeded with either an unpaired t-test or a two-way ANOVA, complemented by Bonferroni's post hoc analysis. In cases of variance non-homogeneity, Welch's t-test and Welch ANOVA tests with Dunnett T3 post hoc analysis were applied.

To calculate the relative gene expression levels, the  $2^{-\Delta\Delta C_t}$  method was utilized, with gene expression quantified in terms of fold change against GAPDH. This relative level of mRNA expression was assessed by comparing the experimental to the control levels.

All statistical tests were two-tailed with a type I error rate fixed at  $\alpha = 0.05$ . Experimenters remained unaware of group assignments and outcomes throughout the research. *P*-values below 0.05 were deemed significant, with significance thresholds set at \**P* < 0.05, \*\* *P* < 0.01, \*\*\* *P* < 0.001, \*\*\*\* *P* < 0.0001.

### Results

#### Tregs in PB and lung tissue are reduced among IPF patients

We analyzed gene expression profiles from the GEO database including GSE28221, GSE33566, and GSE15197, which contain IPF samples and healthy controls to estimating immune infiltration. Tregs score was significantly decreased in IPF (Fig. 2a). CD25/IL2RA was significantly decreased in IPF in both array data and sequencing data (Fig. 2b-c). The Tregs-associated negative marker gene CD127 was significantly increased in IPF in the sequencing data (Fig. 2d).

PB was collected from healthy individuals and patients diagnosed with IPF (Fig. 2e). The concentrations of fibrosis-related proteins in the PB were determined by ELISA. IPF patients had significantly higher levels of HAase and LN-5 in serum compared to health individuals (Fig. 2f). The relative mRNA expressions of genes associated with Th1 (IFN- $\gamma$  and TNF- $\alpha$ , Fig.S1a-b), Th17 (Fig.S1c), and Tregs were determined by qPCR (IL-10, Foxp3

and CTLA4, Fig. 2g-i). The mRNA expression levels of Tregs-related genes in the PBMCs of IPF patients were significantly lower compared with the healthy persons. Consistently, the FCM analysis also found the percentage of Tregs present in the PB of IPF patients was markedly lower than that of healthy individuals (Fig. 2j-k), whereas there was no significant difference in the proportions of Th1 and Th17 (Fig.S1d-f). Between the expressions of HAase and the proportion of Tregs, we performed a correlation analysis, which showed a negative correlation (Fig. 2l). Immunofluorescence staining results showed that the number of Tregs in the lung tissue of IPF patients also exhibited a statistically significant decrease compared to healthy individuals (Fig. 2m-n).

#### Tissue heterogeneity of MSCs in regulating Tregs differentiation

MSCs derived from various tissue sources have significant tissue heterogeneity. In our previous study, two strains of UCMSCs that differed in their ability to regulate Tregs differentiation were used to treat liver fibrosis and the therapeutic efficacy was proportional to the Tregs regulatory capacity [17]. When these two strains of UCMSCs were applied to the treatment of IPF mouse models, they also exhibited the same efficacy correlation (Fig. S2). We manufactured eight types of MSCs from various tissue sources in accordance with the requirements of current GMP guidelines. All strains of MSCs used in this study were strictly evaluated their surface markers, biological characteristics, and microbial contamination, in line with the basic criteria of biological products. The surface marker expression of the MSCs were determined by FCM (Table S2). All types of MSCs consistently expressed high levels of positive surface markers, including CD73, CD90 and CD105 (over than 95%), while displaying minimal expression of negative surface markers, such as CD45, CD14, CD19, CD34, and HLA-DR (less than 2%). Representative flow cytometric phenotyping data for UCMSCs and DMSCs are presented in Fig. S3a. All types of MSCs had multilineage potentials of osteogenic, adipogenic, and cartilage differentiation and representative multilineage differentiations of UCMSCs and DMSCs were confirmed through

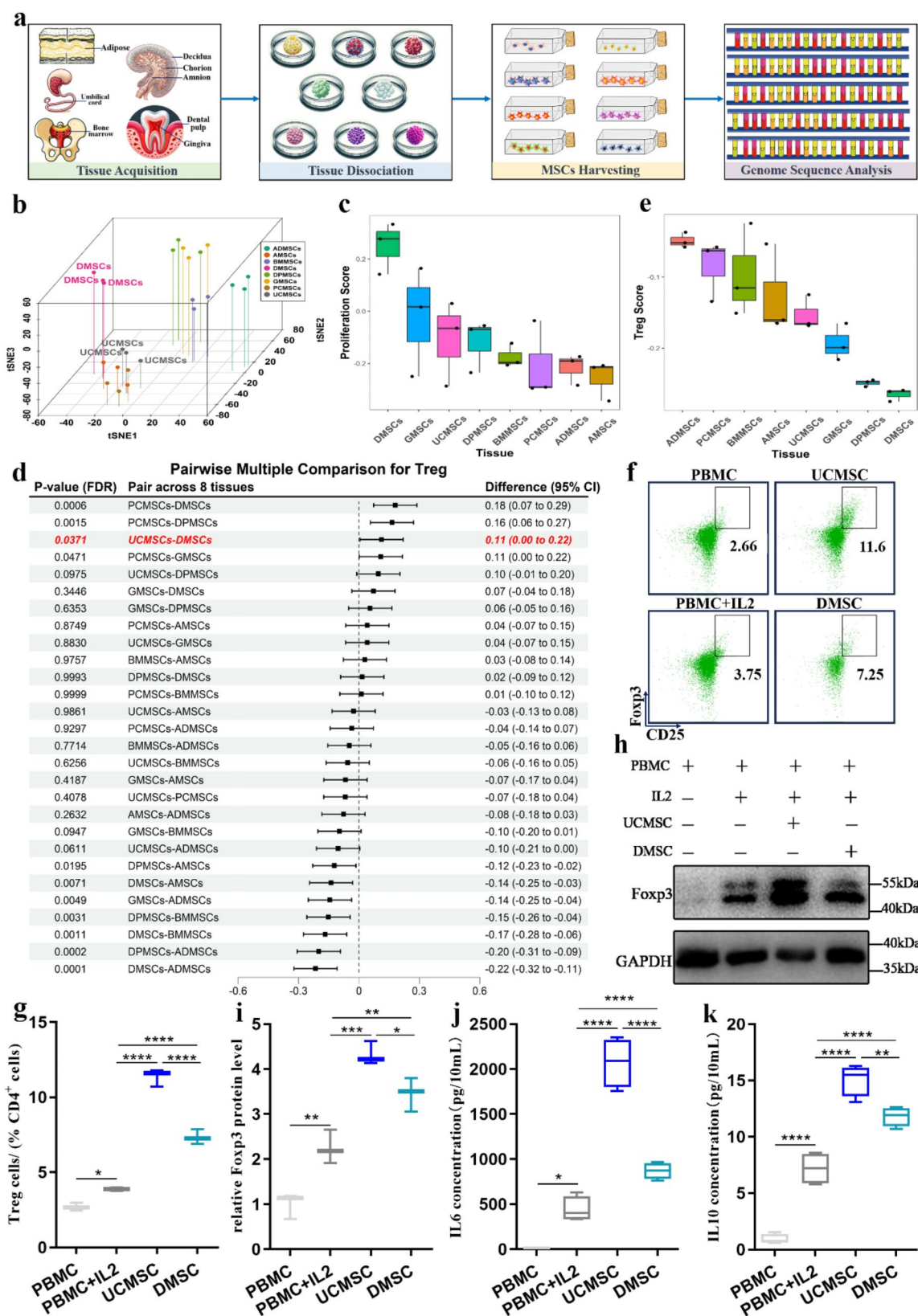


**Fig. 3** (See legend on next page.)

(See figure on previous page.)

**Fig. 3** Bioinformatics reveals tissue heterogeneity of MSCs in regulating Tregs differentiation capability. **(a)** Schematic diagram of the acquisition and detection of MSCs from eight tissue sources. **(b)** The cluster analysis, t-distributed stochastic neighbor embedding analysis of gene expression of 24 samples from eight tissues, supported the heterogeneity of mesenchymal stromal cell. **(c)** Box plot of proliferation comparison of mesenchymal stromal cell across eight tissues. **(d)** Forest plot of multiple comparisons across eight tissues for Tregs. **(e)** Box plot of Tregs-infiltrated fraction comparison of mesenchymal stromal cell across eight tissues. **(f-g)** UCMSC and DMSC were co-cultured with PBMCs induced by IL-2, and the percentage of Tregs was determined by flow cytometric analysis. **(h-i)** The protein levels of the Tregs marker Foxp3 were detected by western blotting and quantified in each group. **(j-k)** The levels of Tregs related cytokines IL10 and IL6 in the supernatants of each group were determined by CBA kit. Images of unedited full blots in Figure S8

Alizarin Red, Oil red O, and Alcian Blue staining, respectively (Fig. S3b). Collectively, our established MSCs met the clinic criteria for MSC identification.

To screen out optimal subtype of MSCs which targeted to the Tregs differentiation regulation in IPF patients, the above eight types of MSCs derived from different tissues were performed RNA-seq analysis (Fig. 3a). The basic genetic visualization of genes was achieved by t-SNE (t-distributed stochastic neighbor embedding), the non-linear dimension reduction method that clusters samples with similar expression patterns. The results showed both inter-organizational and intra-organizational heterogeneities in the samples (Fig. 3b). The ssGSEA was used to quantify the infiltrate levels of four T cell immune signatures for each sample with expression data. Through significant enrichment analysis of the KEGG pathway, we examined the biological roles of genes expressed differentially. We assessed the enrichment of diverse gene sets across eight tissues utilizing ANOVA, followed by multiple comparisons executed via Tukey's honestly significant difference method. The results indicated that DMSCs, GMSCs, and UCMSCs had higher proliferation scores among the eight types of MSCs (Fig. 3c). A pairwise multiple comparison was conducted to analyze the capacity of eight types of MSCs in regulating Tregs, and the MSCs have been ranked in order of Tregs score, from highest to lowest. Significant differences were found between UCMSCs and DMSCs in their ability to regulate Tregs (Fig. 3d-e).

To validate whether the differential regulation of Tregs differentiation is consistent with the sequencing results, UCMSCs and DMSCs were co-cultured with PBMCs and their ability to immunomodulate Tregs, Th1, and Th17 were assessed by flow cytometric analysis. Upon IL-2 stimulation, UCMSCs significantly increased the percentage of anti-inflammatory Tregs derived from co-cultured PBMCs compared with DMSCs (Fig. 3f-g). UCMSCs coculture also markedly increased the expression levels of Tregs-related cytokines (IL6 and IL10) and proteins (Foxp3) compared with DMSCs coculture (Fig. 3h-k). Both UCMSCs and DMSCs could down-regulated the pro-inflammatory subsets of the Th1 and Th17 population differentiation derived from co-cultured PBMCs upon cocktail stimulation (Fig. S3c-d), but without significant difference. These results confirmed the different Tregs-regulatory capacities between UCMSCs and DMSCs by RNA sequencing analysis. Based on these

results, UCMSCs and DMSCs were selected as the therapeutic cells to explore their efficacies in treatment of IPF. To eliminate individual variation, clinic-grade UCMSCs/DMSCs from three donors were mixed in a 1:1:1 ratio, termed UC-Mix/D-Mix, for subsequent experiments.

#### **Tregs induced by MSCs play a critical role in the treatment of IPF, and UCMSCs with higher Tregs-regulatory capacities significantly increase the proportion of Tregs in vivo and improve the therapeutic efficacy of IPF**

To establish the mouse model of IPF, BLM (5 mg/kg) was dissolved in PBS and administered to the mice by tracheal injection. A total of  $5 \times 10^5$  UC-Mix or D-Mix in 300  $\mu$ l PBS were injected intravenously into the tail vein of each mouse at 7 and 14 days after BLM injection. Mice were sacrificed 21 days after BLM injection (Fig. 3a). In the treatment of BLM-induced IPF mice, UC-Mix and D-Mix showed differential therapeutic efficacy. We measured the levels of hydroxyproline, collagen,  $\alpha$ -SMA, and ColI in the lungs. The levels of ColI and  $\alpha$ -SMA in the UC-mix group were lower than in the D-mix group, with statistical significance (Fig. 1b-d). The results showed that, compared to the D-mix, the UC-mix significantly reduced the levels of hydroxyproline and collagen (Fig. 1e-f). These findings indicate that both UCMSCs and DMSCs have therapeutic effects on IPF, but the subtype of MSCs with a high capability of regulating Tregs differentiation has a better repair efficacy. This suggests that the recovery of Tregs homeostasis is closely related to the repair effect on IPF. We determined the proportions of Tregs (CD4<sup>+</sup>CD25<sup>+</sup>Foxp3<sup>+</sup>) in the blood, spleen and thoracic lymph nodes of the BLM-induced IPF mice treated with MSCs. Both UC-Mix and D-Mix treatment could improve the decreased Tregs proportions in blood, spleens and thoracic lymph nodes of BLM-induced IPF mice. In addition, the group treated with UC-Mix exhibited a significant increase in Tregs proportions in all three types of tissue samples compared to the D-Mix treatment group (Fig. 1g-l). To deplete Tregs, PC61 mAb (rat anti-murine CD25 IgG1) was administered in BLM-induced IPF mice treated with UC-Mix. 30  $\mu$ g of purified PC61 antibody was injected intraperitoneally with 200  $\mu$ l of PBS on days 9, 13 and 17 after BLM injection. Rat isotype IgG1 was used as a control (Fig. 3m). After PC61 antibody blockade, the proportion of Tregs in the blood and lymph nodes of the mice was significantly reduced and approached close to zero, indicating Tregs

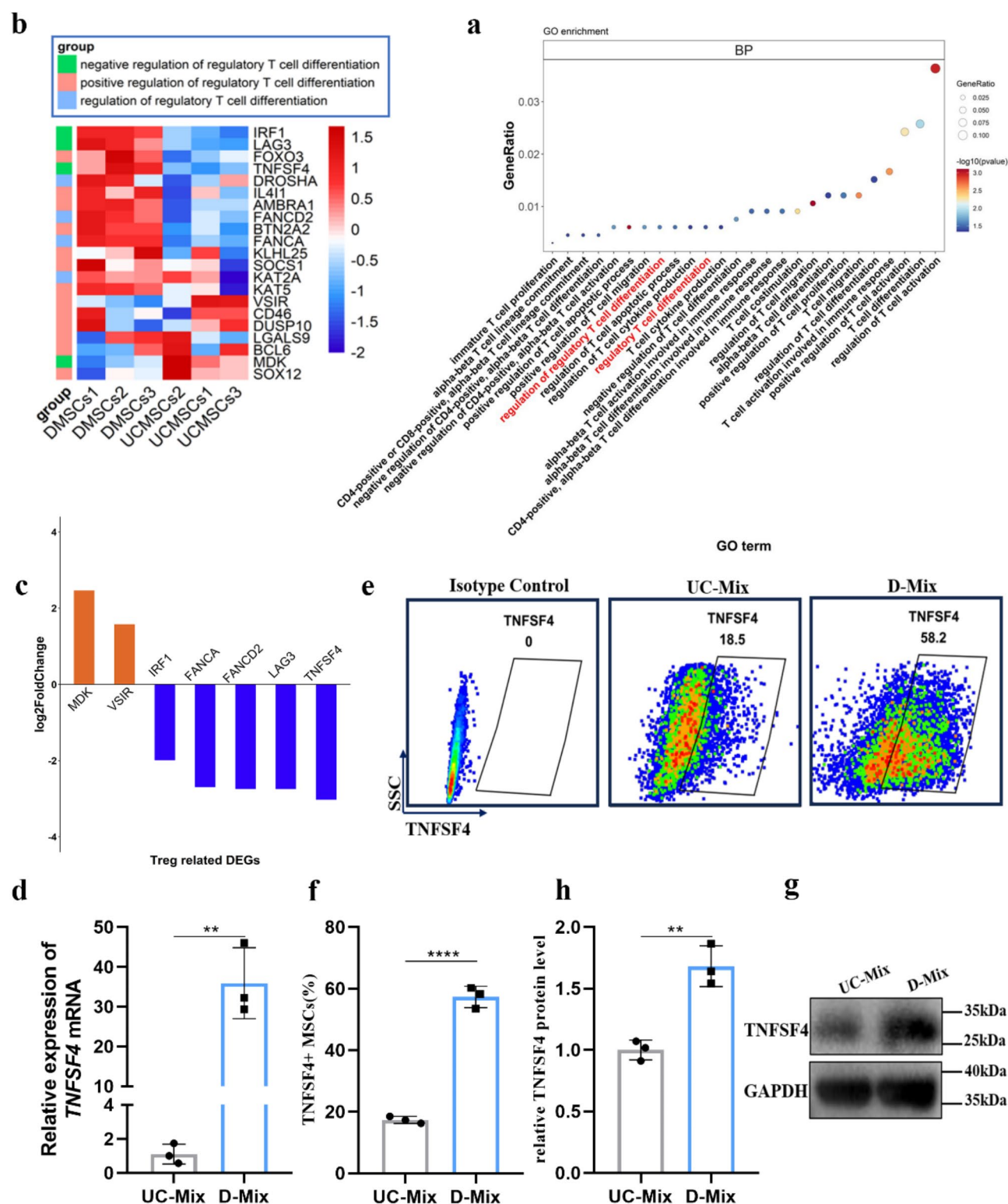


**Fig. 4** (See legend on next page.)



(See figure on previous page.)

**Fig. 4** Bioinformatics data analysis shows that the gene most associated with the heterogeneity of MSCs in regulating Tregs differentiation is *TNFSF4*. **(a)** Bubble plot showing the GO enrichment analysis of immune-related significant pathways of DEGs between UCMSCs and DMSCs, especially enriched in plenty of T cell related pathways. **(b)** Gene expression heatmap showing the expression levels of 21 Tregs-related genes between UCMSCs and DMSCs. The color of each square indicates the scaled expression level of each gene. The columns show each sample, while the rows show each DEGs related to Tregs. **(c)** Bar plot indicates the Tregs-related DEGs between UCMSCs and DMSCs. There was significant difference for *TNFSF4* with the maximal foldchange. Compared to DMSCs, the orange represents Tregs-related genes that are upregulated in UCMSCs, while the blue represents those that are downregulated. **(d)** The expression levels of *TNFSF4* in UC-Mix and D-Mix were determined by qPCR. **(e-f)** The proportion of *TNFSF4*<sup>+</sup> cells in the UC-Mix and D-Mix were determined by flow cytometric analysis. **(g-h)** Protein levels of *TNFSF4* in UC-Mix and D-Mix were determined by western blotting and quantified. Images of unedited full blots in **Figure S9**

were effectively depleted (Fig. 3n-q). In BLM-induced IPF mice, administration of the PC61 antibody significantly eliminated the therapeutic effects of UCMSCs treatment. Hydroxyproline and collagen are increased to pre-treatment levels in the lungs of mice after Tregs depletion (Fig. 3r-s). All the results indicated the recovery of decreased T Tregs proportions played a critical role in rehabilitation of IPF mice after MSCs treatment.

#### ***TNFSF4* associated with heterogeneity of Tregs differentiation regulation between UCMSCs and DMSCs**

Next, we investigated the critical gene was associated with the heterogeneity of Tregs differentiation regulation between UCMSCs and DMSCs. We further analyzed the DEGs between UCMSCs and DMSCs and the biological functions of the DEGs by KEGG significant pathway enrichment analysis. A bubble plot was presented, which displayed the GO enrichment analysis of immune-related significant pathways of DEGs between UCMSCs and DMSCs. The plot showed substantial enrichments in T cell-related pathways, and a significant difference in pathways related to Tregs regulation (Fig. 4a). The heatmap showed the expression levels of 21 Tregs-related genes between UCMSCs and DMSCs (Fig. 4b). The Tregs related DEGs between UCMSCs and DMSCs were listed in a bar chart, among which *TNFSF4* was showed the highest significance with the largest fold changes (Fig. 4c). The mRNA expression level of *TNFSF4* in UC-Mix was significantly lower than that in D-Mix (Fig. 4d). Consistently, the protein level of *TNFSF4* in UC-Mix was remarkably lower than that in D-Mix by FCM and western blotting (Fig. 4e-h). We also examined the gene and protein expression of *TNFSF4* in UCMSC and DMSC strains from different donors and came to the same conclusion, the expression levels of *TNFSF4* were significantly lower in UCMSC strains compared with DMSC strains (Fig. S4a-b).

To investigate whether differential expressions of *TNFSF4* between UCMSCs and DMSCs lead to the discrepancy in Tregs differentiation regulation, we used shRNA-lentivirus targeting *TNFSF4* to knock down the high expression of *TNFSF4* in DMSCs, and lentiviral plasmids encoding *TNFSF4* to overexpress *TNFSF4* in UCMSCs. Three different plasmids were used to knock down *TNFSF4* in DMSCs, of which

*TNFSF4*-shRNA-LV3-1 with the most efficiency of *TNFSF4* knocking-down confirmed by qPCR and western blotting in DMSCs was selected for further experiments (Fig. S4c-d). The lentivirus *TNFSF4*-LV8 is tagged with a RFP, while *TNFSF4*-shRNA-LV3 lentivirus is tagged with a GFP. Therefore, the transfection efficiency was determined by calculating the proportion of transfected MSCs expressing GFP/RFP under a fluorescence microscope 48 h after screening. (Fig. S5a-b).

The expression of *TNFSF4* in D-mix after sh-*TNFSF4* transfection (D-mix-sh-*TNFSF4*) was detected by qPCR, FCM and western blotting, and the results showed that *TNFSF4* was successfully knocked down (Fig. 5a-d). To assess the Tregs differentiation capability of D-mix-sh-*TNFSF4*, we co-cultured them with PBMCs isolated from human bloods. We observed a significant increase in Tregs percentage in D-mix-sh-*TNFSF4* group compared to the D-Mix-sh-LV group (sh RNAi control) (Fig. 5e), and Tregs-related cytokines (IL6 and IL10) were accordingly increased in their supernatants (Fig. 5f-g). The protein levels of Foxp3 were also increased in PBMCs in the D-mix-sh-*TNFSF4* group (Fig. 5h-i). The same assays were also performed on UC-Mix-*TNFSF4* and the overexpression of *TNFSF4* in UCMSCs was confirmed (Fig. 5j-m). We co-cultured UC-Mix-*TNFSF4* with PBMCs and found a decrease in the percentage of Tregs compared to the UC-Mix-LV control group (Fig. 5n). The Tregs-related cytokines (IL6 and IL10) and protein (Foxp3) all were decreased accordingly (Fig. 5p-s). We also tested the effects of D-mix-sh-*TNFSF4* and UC-Mix-*TNFSF4* on Th1/Th17 regulation and found that *TNFSF4* deficiency or over-expression did not significantly influence the differentiations Th1/Th17 (Fig. S5c-f). Taken together, the results supported that *TNFSF4* expression level was associated with heterogeneity of Tregs differentiation regulation between UCMSCs and DMSCs.

#### **The *TNFSF4* expression level was negatively associated with anti-fibrotic activity of MSCs in vitro and in vivo**

After we found *TNFSF4* expression level of MSCs was negatively associated with Tregs differentiation regulation, then we investigated whether *TNFSF4* expression level of MSCs accordingly was attributed to the anti-fibrotic activity. In vitro, fibrosis cell model was induced by TGF- $\beta$ 1 stimulation in Hef cells and the expressions

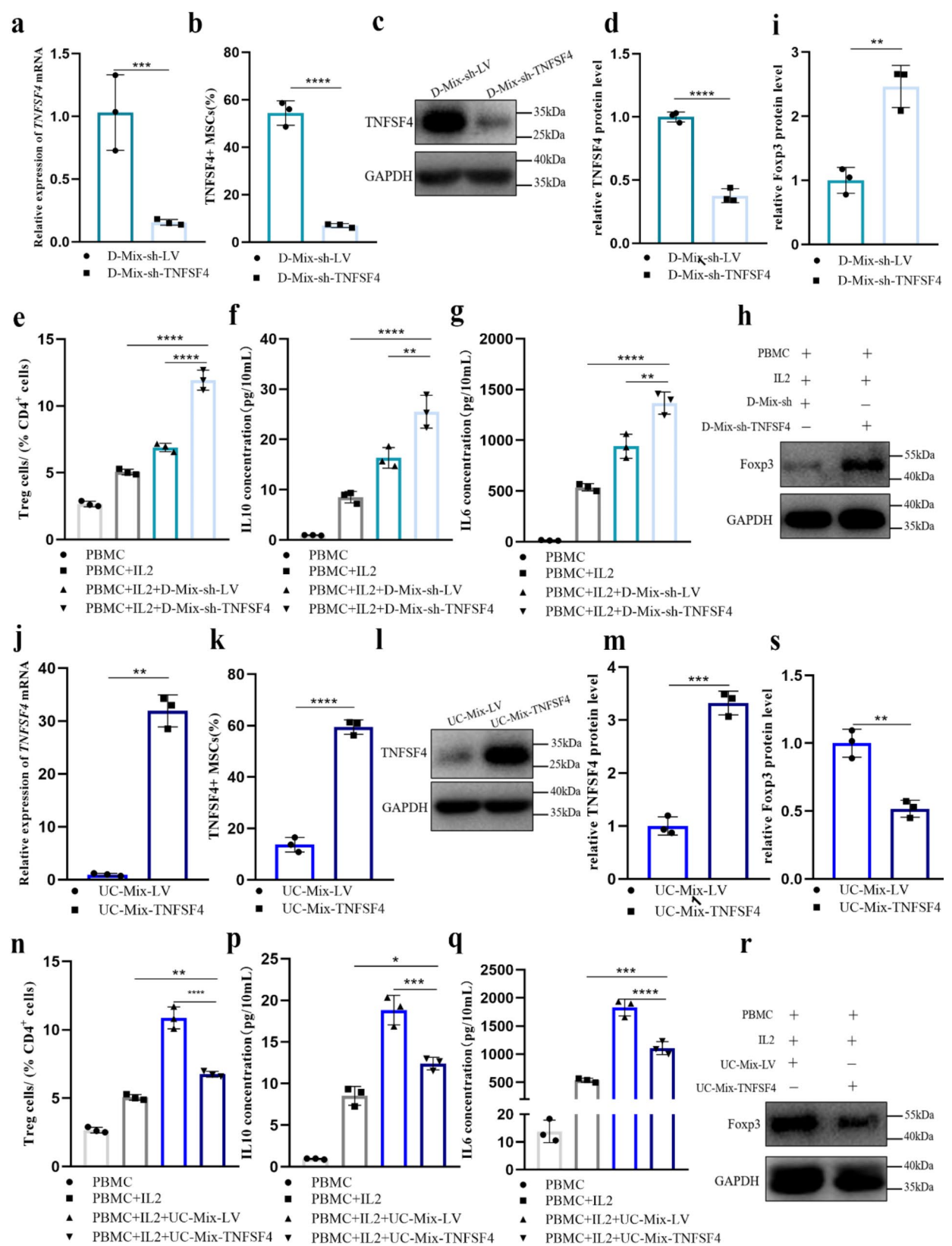


**Fig. 5** (See legend on next page.)

(See figure on previous page.)

**Fig. 5** Gene editing technology demonstrate that the most significant gene associated with the heterogeneity of MSCs in regulating Tregs differentiation is TNFSF4. **(a)** Using virus plasmid transfection for gene knockout technology, the TNFSF4 gene in D-Mix cells was knocked out, and the stable cell line after puromycin selection was named D-Mix-sh-TNFSF4. The control group D-Mix cells were transfected with only the empty vector virus plasmid, and the stable cell line after selection was named D-Mix-sh-LV. QPCR to determine the mRNA expression of *TNFSF4* in D-Mix-sh-TNFSF4 and D-Mix-sh-LV. **(b)** The proportion of TNFSF4<sup>+</sup> MSCs in D-Mix-sh-TNFSF4 by flow cytometric analysis. **(c-d)** Protein levels of TNFSF4 in D-Mix-sh-TNFSF4 were determined by western blotting and quantified. **(e)** D-Mix-sh-TNFSF4 were co-cultured with PBMCs induced by IL-2, and the percentage of Tregs was determined by flow cytometric analysis. **(f-g)** The levels of Tregs related cytokines IL10 and IL6 in the supernatants of each group were determined by CBA kit. **(h-i)** The protein levels of the Tregs marker Foxp3 were detected by western blotting and quantified in each group. **(j-s)** Through virus plasmid transfection and gene over-expression technology, the TNFSF4 gene was overexpressed in UC-Mix cells, and the stable cell line after puromycin selection was named UC-Mix-TNFSF4. For the control group UC-Mix cells, only the empty vector virus plasmid was transfected, and the stable cell line after selection was named UC-Mix-LV. The experiments described in this figure, i-t, were conducted on both UC-Mix-TNFSF4 and UC-Mix-LV cell lines. Images of unedited full blots in Figure S10

of fibrotic proteins such as  $\alpha$ -SMA and Col I in Helf cells were determined. The supernatants from PBMCs co-cultured with different MSCs (including UC-Mix-LV, UC-Mix-TNFSF4, D-Mix-sh-LV, and D-Mix-sh-TNFSF4) were added to the TGF- $\beta$ 1-stimulated Helf cells. The results demonstrated that TNFSF4 knock-down improved the anti-fibrotic activity of D-MSCs in TGF- $\beta$ 1-stimulated Helf cells and TNFSF4 over-expression significantly blocked the anti-fibrotic activity of UC-MSCs (Fig. S6a-b). Consistent with the in vitro results, MSCs with lower TNFSF4 expression had better therapeutic outcomes when applied to BLM-induced IPF mice (Fig. S6c-d).

#### MSCs precisely modulating the subpopulations of Tregs via TNFSF4-TNFRSF4 axis

Following a comprehensive series of experiments validating the inverse correlation between MSCs' Tregs modulatory capabilities and their TNFSF4 expression levels, we postulate that MSCs exhibiting diminished TNFSF4 expression may lead to reduced binding to TNFRSF4 ligands on immune cells. Consequently, this attenuation could inhibit the TNFSF4-TNFRSF4 pathway, which negatively regulates Tregs differentiation. Consequently, a cascade effect ensues, culminating in heightened expression and differentiation of Tregs-associated factors, thereby fostering enhanced therapeutic efficacy in treating IPF. To substantiate this hypothesis, we conducted mechanistic investigations within IL-2-induced PBMCs and D-Mix co-culture systems, augmented with diverse monoclonal antibodies targeting the TNFSF4-TNFRSF4 pathway blockade. Notably, administration of Oxelumab (anti-TNFSF4 monoclonal antibody), Telazorlimab (anti-TNFSF4 monoclonal antibody), or Amlitelimab (anti-TNFRSF4 monoclonal antibody) significantly elevated Tregs proportions (Fig. 6a-b). These findings corroborated the proposed inference regarding the inhibitory effect of the TNFSF4-TNFRSF4 negative regulatory pathway.

It is widely recognized that Tregs, characterized by their immunosuppressive properties, play a pivotal role in maintaining immune tolerance and homeostasis within immune responses [41]. Recent investigations

have unveiled the heterogeneity inherent within these classically defined Tregs, delineating distinct functional and phenotypic subsets including quiescent Tregs (rTregs), activated Tregs (aTregs), and cytokine-secreting non-suppressive Tregs [42]. Consequently, our endeavor aims to delve deeper into the correlation between MSC-derived TNFSF4 and the equilibrium, subtypes, and proliferative capacity of Tregs subpopulations. This endeavor seeks to discern the specific Tregs subgroups or subtypes regulated by MSCs via TNFSF4-TNFRSF4 axis, thereby augmenting the efficacy of therapeutic interventions in IPF. MSCs co-cultivated with IL2-induced PBMCs exhibited a marked elevation in the proportion of aTregs (CD4<sup>+</sup> CD25<sup>+</sup> CD38<sup>+</sup> HLA-DR<sup>+</sup>) within the UC-Mix group compared to the D-Mix group (Fig. S7a-b). Given the heterogeneous composition of immune cells within PBMCs and the imperative to delineate the precise target cells modulating Tregs differentiation by MSCs, we adopted a methodology of magnetic bead separation to isolate and enrich purified CD4<sup>+</sup> T cells from PBMCs in blood. Subsequently, we executed the aforementioned experimental paradigm, yielding congruent outcomes (Fig. 6c-d). Additionally, meticulous scrutiny was conducted on the mRNA and protein expression levels of Tregs subtype-associated genes (Foxp3, GTIR, and Helios) across each experimental group. Notably, a discernible upsurge in Foxp3 and GTIR expression was observed within the UC-Mix cohort, whereas Helios exhibited unaltered levels (Fig. 6e-i). These discernments intimate that TNFSF4 within MSCs may selectively orchestrate the regulation of distinct Tregs subtypes. Analogously, commencing with the co-cultivation of UC-mix/D-mix alongside IL2-induced PBMCs, an examination of the percentage distribution of each Tregs subtype ensued. Evaluation of these samples encompassed an analysis of CD4, CD25, CD45RA, and CCR7 expressions. Within this co-culture milieu, UC-Mix evinced a substantial augmentation in the proportions of Treg<sup>CM</sup> (CD4<sup>+</sup> CD25<sup>+</sup> CCR7<sup>+</sup> CD45RA<sup>-</sup>) and Treg<sup>E</sup> (CD4<sup>+</sup> CD25<sup>+</sup> CCR7<sup>+</sup> CD45RA<sup>+</sup>), while the ratios of Treg<sup>EM</sup> (CD4<sup>+</sup> CD25<sup>+</sup> CCR7<sup>-</sup> CD45RA<sup>+</sup>) and Treg<sup>naïve</sup> (CD4<sup>+</sup> CD25<sup>+</sup> CCR7<sup>-</sup> CD45RA<sup>-</sup>) remained unaltered. UC-Mix, distinguished by diminished TNFSF4 levels, exhibited a

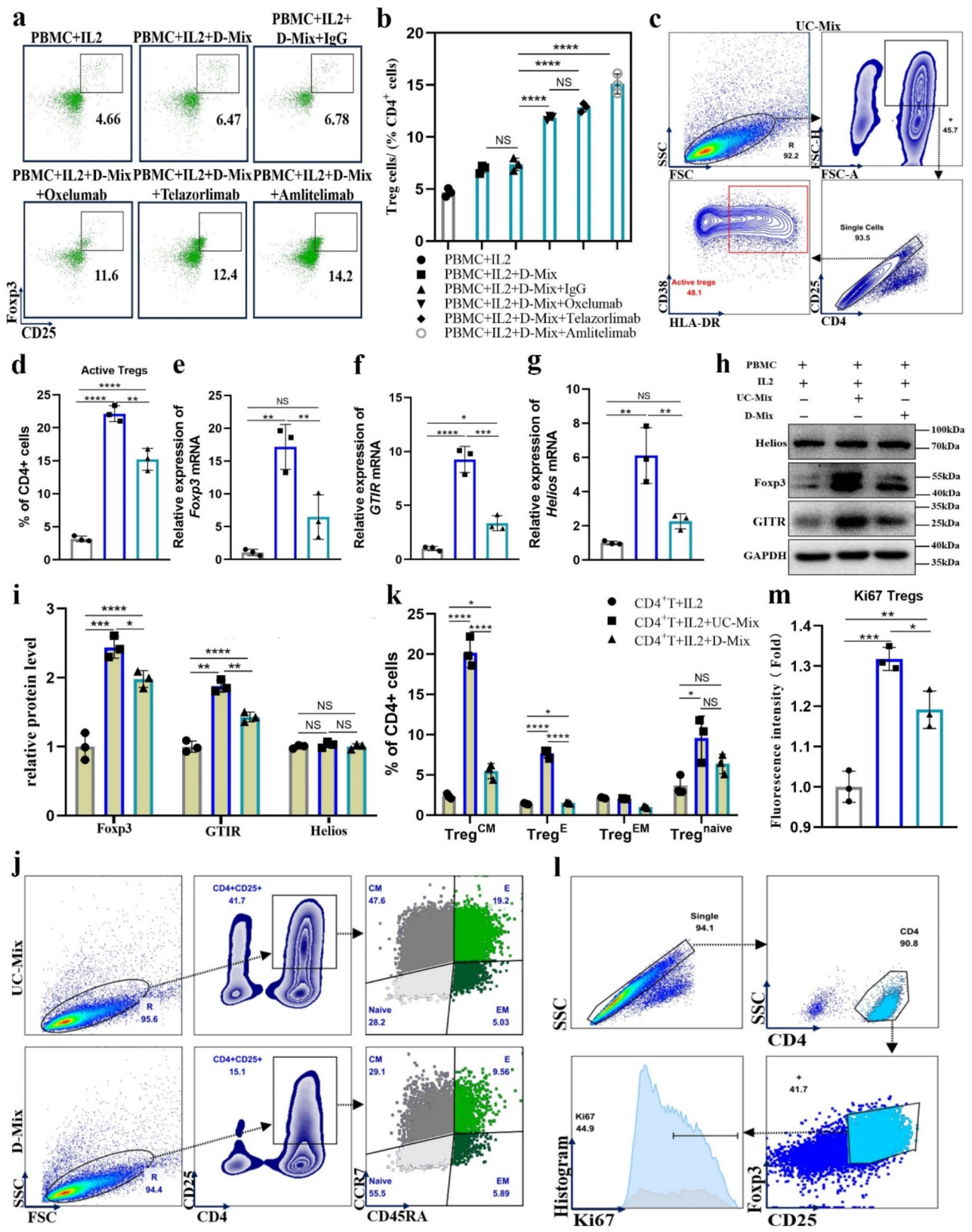


Fig. 6 (See legend on next page.)



(See figure on previous page.)

**Fig. 6** MSCs regulate the differentiation, subtype distribution, and proliferation of Tregs subpopulations through the TNFSF4-TNFRSF4 axis. **(a-b)** Flow cytometric analysis of Tregs after addition of Oxelumab (anti-TNFSF4), Telazolimab (anti-TNFSF4) and Amlitelimab (TNFRSF4) to the D-Mix and PBMCs co-culture systems. Contour plots showing the cell populations from the indicated gates. The percentage of Tregs (CD4<sup>+</sup> CD25<sup>+</sup> Foxp3<sup>+</sup>). **(c-d)** UC-Mix/D-Mix were co-cultured with purified CD4<sup>+</sup> T cells induced by IL2. The proportion of activated Tregs (CD4<sup>+</sup> CD25<sup>+</sup> CD38<sup>+</sup> HLA-DR<sup>+</sup>) was determined by FCM. **(e-g)** The relative mRNA expression levels of Tregs subtype-related genes (*Foxp3*, *GTIR* and *Helios*) in each group were determined by qPCR. **(h-i)** The expression levels of Tregs subtype-associated proteins (Foxp3, GTIR and Helios) in each group were determined by western blotting. **(j-k)** UC-Mix/D-Mix were co-cultured with purified CD4<sup>+</sup> T cells induced by IL2 and the percentage of each Tregs subtype was determined by FCM. The samples were analyzed for the expression of CD4, CD25, CD45RA and CCR7. Contour plots showing the cell populations from the indicated gates. The proportions of Treg<sup>CM</sup>, Treg<sup>E</sup>, Treg<sup>EM</sup> and Treg<sup>naive</sup> were counted. **(l-m)** FCM was used to analyze the proliferation of Tregs in each group. Representative FCM gating strategy correspond to Tregs (CD4<sup>+</sup> CD25<sup>+</sup> Foxp3<sup>+</sup>), and proliferated Tregs gating was further stratified by the expression of Ki67. The proportions of Ki67 Tregs were counted. Images of unedited full blots in Figure S11

more robust modulation of Treg<sup>CM</sup> and Treg<sup>E</sup> subtypes, in contrast to Treg<sup>EM</sup> and Treg<sup>naive</sup> subtypes (Fig. S7c-d). Replication of these investigations with purified CD4<sup>+</sup> T cells yielded consistent findings in Tregs subtype regulation (Fig. 6j-k). Furthermore, the proliferative activity of Tregs was evaluated by analyzing the proportion of Ki67<sup>+</sup> Tregs. Intriguingly, UC-Mix notably fostered Tregs proliferation relative to D-Mix (Fig. 6l-m, and Fig. S7e-f). In summary, MSCs evincing reduced TNFSF4 expression substantially modulate Tregs activation, subtypes, and proliferation.

## Discussion

By integrating multiple array datasets from GEO and merging samples, we analyzed the immune cell characteristics and infiltration features of 186 IPF patients and 62 healthy individuals. Our preliminary findings revealed distinct characteristics of Tregs immune cells. Our study reveals a significant decrease in Tregs in both the PBMCs and lung tissues of IPF patients compared to healthy individuals. It is imperative to underscore the pivotal role of MSCs, renowned for their formidable immunomodulatory prowess. These cells promote the transdifferentiation of other immune cells into Tregs, impacting the immune microenvironment and offering therapeutic benefits [43]. Intriguingly, this study, alongside our preliminary investigations, unearthed that MSCs exhibiting augmented Tregs regulatory capabilities manifested a pronounced anti-fibrotic action (Fig.S1) [17]. Nonetheless, the mechanisms underpinning the heterogeneity in the MSC-mediated Tregs modulation remain to be elucidated. Leveraging our Stem Cell Center, we procured MSCs from eight tissue types (sourced from three donors each) and subjected them to comprehensive whole-genome sequencing. Through meticulous cluster analysis, the enrichment analysis of immune-related significant pathways, and the comparative assessment of Tregs infiltration scores, we discerned that lower TNFSF4 expression in MSCs correlates with better Tregs regulation. This supports previous findings that TNFSF4-TNFRSF4 signaling reduces Tregs generation by fostering the proliferation of T cells [44]. Our research confirms this signaling in MSCs and identifies a new MSC subtype with

low TNFSF4 expression, improving Tregs generation, activation (CD38<sup>+</sup>HLA-DR<sup>+</sup>) and proliferation (Ki67<sup>+</sup>). This subtype not only augments the genesis of Tregs subpopulations but also enhances Tregs, thereby recalibrating the distribution of Tregs subtypes. This breakthrough advances our knowledge of MSC immunoregulation and its therapeutic potential for fibrosis.

Stem cell research faces a key challenge due to limited cellular resources, hindering comparisons of different cell types' effectiveness against specific diseases and understanding treatment variability. Presently, using the same type of MSCs for various diseases is problematic, as it fails to consider each disease's unique causes and changes, making this one-size-fits-all approach flawed [45]. Our investigation, has unearthed a significant negative correlation between the proportion of Tregs in the blood of IPF patients and the fibrosis marker HAase, insinuating the contributory role of Tregs deficiency in the advancement of fibrosis. A burgeoning corpus of evidence accentuates the pivotal role of the equilibrium between Tregs and pro-inflammatory cells, such as Th1 and Th17 cells, in delicately modulating the dichotomy between alveolar repair and fibrogenesis [22]. The inherent ability of MSCs to ameliorate the imbalance between Th17 and Tregs, alongside their capacity to foster the differentiation of type II alveolar epithelial cells and augment epithelial damage repair, heralds a promising avenue for the amelioration of pulmonary fibrosis [46]. While there's growing agreement on the effectiveness of MSCs in treating IPF by modulating Tregs levels [7, 47], identifying the best MSCs for this purpose remains unclear. Our research shows that changes in TNFSF4 expression within MSCs directly impact their ability to regulate Tregs and affect the production of fibrosis-related cytokines, IL6 and IL10 [48, 49], highlighting its importance in fibrosis severity. We've demonstrated TNFSF4's crucial role in MSCs' influence on Tregs differentiation, activation, and proliferation, and how the TNFSF4-TNFRSF4 signaling pathway facilitates MSC-immune cell interactions. By blocking TNFSF4 on MSCs and TNFRSF4 on inflammatory cells, we saw an increase in Tregs differentiation. This challenges previous beliefs that TNFSF4 is mainly expressed on antigen-presenting

cells, including B cells, macrophages, and dendritic cells [50–52], showing its significant presence on MSCs. This suggests TNFSF4's signaling is vital for T cell viability during their late proliferation and effector phases, enhancing our understanding of MSCs' immunomodulatory effects.

Our study highlights Tregs' essential role in MSC therapy for IPF in mice, showing that MSC administration increases Tregs systemically and is crucial for the therapy's anti-fibrotic effect. This effect is significantly reduced when Tregs are depleted through anti-CD25 antibody-mediated blockade, emphasizing their critical role in treatment [53]. Research has shown that Tregs levels [18], which are vital for controlling the body's autoimmune response and are diminished in pulmonary fibrosis, correlate with disease severity. Similarly, MSCs have been shown to increase Tregs levels in liver fibrosis, promoting an immune-tolerant state and improving liver health [24]. Our investigations unveil a pronounced negative correlation between the expression levels of TNFSF4 in MSCs and the systemic Tregs levels, alongside the therapeutic impact on fibrosis. Through viral transfection methodologies aimed at either silencing or overexpressing TNFSF4 expression, we noted a negligible influence on Th1 and Th17 cells *in vitro*. In contrast, there was a substantial modulation of the Tregs subset proportions and the expression profiles of fibrosis-associated proteins and cytokines, culminating in significant fibrosis alteration *in vivo*. This supports Piconese S, et al.'s theory that TNFSF4 acts as a co-stimulatory molecule, reducing Tregs effectiveness and promoting their differentiation into other immune cells [54].

There are some limitations in present study. Although this study utilized multiple public datasets to analyze the immune characteristics of IPF patients, the sample size of patients is relatively limited and their heterogeneity may still impact the generalizability of the results. Our study has definitely demonstrated the effects of TNFSF4<sup>low</sup>-MSCs in regulating Tregs and exhibiting anti-fibrotic properties in a IPF mouse model, we need to further verify the anti-fibrotic efficacy of TNFSF4<sup>low</sup>-MSCs in IPF patients. So, we next plan to use clinic-grade TNFSF4<sup>low</sup>-MSCs to treat IPF patients in clinic trials, promoting our findings to translational research.

Furthermore, our research confirms that central memory and effector Tregs subtypes play key roles in combating fibrosis, unlike effector memory and naive Tregs. This aligns with prior assertions regarding the constitutive expression of its ligand TNFSF4 on inflammatory cells, with potential implications for late-stage cellular proliferation and effector functionality, thereby enriching our comprehension of the immunological underpinnings critical to fibrosis progression and therapeutic intervention.

## Conclusions

Traditionally, the immunosuppressive and tissue regenerative capacities of MSCs were attributed to their paracrine functions, characterized by the secretion of a plethora of cytokines, chemokines, and growth factors [55]. However, our research elucidates a novel immunoregulatory mechanism employed by MSCs, involving the precise modulation of Tregs subpopulations through direct cell surface protein interactions with immune cells. Moreover, we have identified a pivotal membrane protein pivotal in this Tregs subpopulation regulation, establishing a direct correlation with the efficacy of IPF treatment. This discovery offers a quantitative metric for the selection of superior IPF therapeutic cells among MSCs derived from various tissue origins and donor sources. In summary, originating from the pressing clinical needs for stromal cell therapies, our research transcends the prevailing limitations associated with employing a uniform stromal cell type across multiple disease treatments without foundational selection criteria and quality benchmarks.

## Abbreviations

ADMSCs	Adipose-derived MSCs
AMSCs	Amniotic MSCs
aTregs	Activated Tregs
BLM	Bleomycin
BMMSCs	Bone marrow-derived MSCs
CBA	Cytometric Beads Assay
cGMP	Current Good Manufacturing Practice
DAPI	4',6-diamidino-2-phenylindole
DEGs	Differentially expressed genes
D-mix-sh-TNFSF4	D-mix after sh-TNFSF4 transfection
DMSCs	Decidua MSCs
DPMSCs	Dental pulp-derived MSCs
FBS	Fetal bovine serum
FDR	False discovery rate
GEO	Gene Expression Omnibus
GFP	Green fluorescent protein
GMSCs	Gingival-derived MSCs
Helf	Human fetal lung fibroblasts
IPF	Idiopathic pulmonary fibrosis
MOI	Multiplicity of infection
MSCs	Mesenchymal stromal cells
PB	Peripheral blood
PBMCs	Peripheral blood mononuclear cells
PBS	Phosphate-buffered saline
PCMSCs	Placental villous MSCs
PMA	Phorbol 12-myristate 13-acetate
RFP	Red fluorescent protein
rTregs	Quiescent Tregs
Th	T-helper cells
TNFSF4	Tumor necrosis factor superfamily member 4
TNFSF4 <sup>low</sup> -MSCs	MSCs characterized by low TNFSF4 expression
TPM	Transcripts Per Million
Tregs	Regulatory T cells
t-SNE	t-distributed stochastic neighbor embedding
UCMSCs	Umbilical cord-derived MSCs

## Supplementary Information

The online version contains supplementary material available at <https://doi.org/10.1186/s13287-025-04313-6>.

## Supplementary Material 1

**Acknowledgements**

The authors thank all the tissue donors for MSCs in this study for their collaborative participations. The authors declare that they have not use AI-generated work in this manuscript.

**Author contributions**

YyX and QY were responsible for the design and implementation of the study. They conducted data analysis, visualization, and wrote the initial draft of the manuscript. YrF and YpW provided assistance in preparing MSCs, while LdW aided in carrying out the animal experiments. YyX and YJ has directly accessed and verified the underlying data reported in the manuscript. CwX provided assistance in the implementation of the study. YyX and HY provided part of the foundation and financial support. BW and YwZ were responsible for the study's design and supervision. They also reviewed and revised the manuscript, and provided the necessary foundation and financial support. All authors read and approved the final manuscript.

**Funding**

This study was supported by National Natural Science Foundation of China [No. 82070459, and 82270701 (Bin Wang), and 82270076 (Yingwei Zhang)], Nanjing Municipal Health Science and Technology Development Special Fund Project [No. YKK23108 (Yuanyuan Xie)], Natural Science Foundation of Jiangsu Province of China [No. BK20230141 (Hui Yang)], Clinical Research Special Fund of Nanjing Drum Tower Hospital [No. 2024-LCYJ-PY-77 (Yuanyuan Xie)]. No. BK20230141 (Hui Yang), No. 82070459, and 82270701 (Bin Wang) are responsible for the purchase of study materials including experimental reagents, consumables, etc. No. 82270076 (Yingwei Zhang), No. 2024-LCYJ-PY-77 (Yuanyuan Xie) and No. YKK23108 (Yuanyuan Xie) undertakes the recruitment of patients and healthy volunteers.

**Data availability**

The raw data underpinning the conclusions of this paper will be provided by the authors to any qualified researcher without undue reservation. The raw sequence data reported in this paper have been deposited in the Genome Sequence Archive (Genomics, Proteomics & Bioinformatics 2021) in National Genomics Data Center (Nucleic Acids Res 2024), China National Center for Bioinformation / Beijing Institute of Genomics, Chinese Academy of Sciences (GSA-Human: HRA009484) that are publicly accessible at <https://ngdc.cncb.ac.cn/gsa-human>.

**Declarations****Ethics approval and consent to participate**

Ethnic approval was granted by the Medical Ethics Committees of Nanjing Drum Tower Hospital (Project title: Utilization of Clinical Patient Samples (Tissue/Blood/Body Fluids) and Aborted Fetal Tissue to Extract Stromal Cells for Basic and Clinical Research in Regenerative Medicine and Treatment of Clinical Diseases; Approval No. 2017-161-08; Date of approval: 2017-11-30. Project title: TNFSF4(low)-MSCs Improve IPF by Regulating Tregs Subtypes; Approval No. 2023-675-01; Date of approval: 2023-03-20). All experiments involving mice were approved by the Ethics Committee of Nanjing Drum Tower Hospital (Project title: Research on the Mechanism of MSCs in Treating Pulmonary Fibrosis; Approval No. DWSY-22047178; Date of approval: 2022-04-07). All participants provided written informed consent before enrollment in the study.

**Consent for publication**

Not applicable.

**Competing interests**

The authors declare that they have no competing interest.

**Author details**

<sup>1</sup>Clinical Stem Cell Center, Nanjing Drum Tower Hospital, Affiliated Hospital of Medical School, Nanjing University, Nanjing, Jiangsu 210009, China

<sup>2</sup>Department of Respiratory and Critical Care Medicine, Nanjing Drum Tower Hospital Clinical College of Nanjing University of Chinese Medicine, Nanjing, Jiangsu 210000, China

<sup>3</sup>Clinical Stem Cell Center, Nanjing Drum Tower Hospital, Clinical Medical College of Traditional Chinese and Western Medicine, Nanjing University of Chinese Medicine, Nanjing, Jiangsu 210009, China

<sup>4</sup>School of Life Science, Nanjing University, Nanjing, Jiangsu, China

<sup>5</sup>Department of Respiratory and Critical Care Medicine, Nanjing Drum Tower Hospital, Affiliated Hospital of Medical School, Nanjing University, Nanjing, Jiangsu 210000, China

<sup>6</sup>Jiangsu Key Laboratory for Molecular Medicine, Nanjing University, Nanjing, Jiangsu, China

Received: 9 December 2024 / Accepted: 4 April 2025

Published online: 20 April 2025

**References**

1. du Bois RM. Idiopathic pulmonary fibrosis: present Understanding and future options. *Eur Respiratory Review: Official J Eur Respiratory Soc*. 2011;20(121):132–3.
2. Raghu G, Remy-Jardin M, Myers JL, Richeldi L, Ryerson CJ, Lederer DJ, et al. Diagnosis of idiopathic pulmonary fibrosis. An official ATS/ERS/JRS/ALAT clinical practice guideline. *Am J Respir Crit Care Med*. 2018;198(5):e44–68.
3. Richeldi L, Collard HR, Jones MG. Idiopathic pulmonary fibrosis. *Lancet*. 2017;389(10082):1941–52.
4. George PM, Patterson CM, Reed AK, Thillai M. Lung transplantation for idiopathic pulmonary fibrosis. *Lancet Respir Med*. 2019;7(3):271–82.
5. Tzouveleakis A, Toonkel R, Karampitsakos T, Medapalli K, Ninou I, Aidinis V, et al. Mesenchymal stem cells for the treatment of idiopathic pulmonary fibrosis. *Front Med (Lausanne)*. 2018;5:142.
6. Mazziotta C, Badiale G, Cervellera CF, Tognon M, Martini F, Rotondo JC. Regulatory mechanisms of circular RNAs during human mesenchymal stem cell osteogenic differentiation. *Theranostics*. 2024;14(1):143–58.
7. Tang Z, Gao J, Wu J, Zeng G, Liao Y, Song Z, et al. Human umbilical cord mesenchymal stromal cells attenuate pulmonary fibrosis via regulatory T cell through interaction with macrophage. *Stem Cell Res Ther*. 2021;12(1):397.
8. Hu C, Wu Z, Li L. Mesenchymal stromal cells promote liver regeneration through regulation of immune cells. *Int J Biol Sci*. 2020;16(5):893–903.
9. Liu Z, Wang J, Cheng H, Ke X, Sun L, Zhang QC, et al. Cryo-EM structure of human Dicer and its complexes with a Pre-miRNA substrate. *Cell*. 2018;173(5):1191–e1203112.
10. Yi X, Wei X, Lv H, An Y, Li L, Lu P, et al. Exosomes derived from microRNA-30b-3p-overexpressing mesenchymal stem cells protect against lipopolysaccharide-induced acute lung injury by inhibiting SAA3. *Exp Cell Res*. 2019;383(2):111454.
11. Cargnoni A, Romele P, Bonassi Signoroni P, Farigu S, Magatti M, Vertua E, et al. Amniotic MSCs reduce pulmonary fibrosis by hampering lung B-cell recruitment, retention, and maturation. *Stem Cells Transl Med*. 2020;9(9):1023–35.
12. Huang T, Zhang T, Jiang X, Li A, Su Y, Bian Q, et al. Iron oxide nanoparticles augment the intercellular mitochondrial transfer-mediated therapy. *Sci Adv*. 2021;7(40):eabj0534.
13. Shi L, Han Q, Hong Y, Li W, Gong G, Cui J, et al. Inhibition of miR-199a-5p rejuvenates aged mesenchymal stem cells derived from patients with idiopathic pulmonary fibrosis and improves their therapeutic efficacy in experimental pulmonary fibrosis. *Stem Cell Res Ther*. 2021;12(1):147.
14. Potdar PD, Jethmalani YD. Human dental pulp stem cells: applications in future regenerative medicine. *World J Stem Cells*. 2015;7(5):839–51.
15. Vizoso FJ, Eiro N, Cid S, Schneider J, Perez-Fernandez R. Mesenchymal stem cell secretome: toward cell-free therapeutic strategies in regenerative medicine. *Int J Mol Sci*. 2017;18(9).
16. Lin W, Huang L, Li Y, Fang B, Li G, Chen L, et al. Mesenchymal stem cells and cancer: clinical challenges and opportunities. *Biomed Res Int*. 2019;2019:2820853.
17. Xie Y, Liu S, Wang L, Yang H, Tai C, Ling L, et al. Individual heterogeneity screened umbilical cord-derived mesenchymal stromal cells with high Treg promotion demonstrate improved recovery of mouse liver fibrosis. *Stem Cell Res Ther*. 2021;12(1):359.
18. Kotsianidis I, Nakou E, Bouchliou I, Tzouveleakis A, Spanoudakis E, Steiropoulos P, et al. Global impairment of CD4+CD25+FOXP3+ regulatory T cells in idiopathic pulmonary fibrosis. *Am J Respir Crit Care Med*. 2009;179(12):1121–30.

19. Shimizu Y, Dobashi K, Endou K, Ono A, Yanagitani N, Utsugi M, et al. Decreased interstitial FOXP3(+) lymphocytes in usual interstitial pneumonia with discrepancy of CXCL12/CXCR4 axis. *Int J Immunopathol Pharmacol*. 2010;23(2):449–61.
20. Whitehouse GP, Hope A, Sanchez-Fueyo A. Regulatory T-cell therapy in liver transplantation. *Transpl Int*. 2017;30(8):776–84.
21. Wen J, Zhou Y, Wang J, Chen J, Yan W, Wu J, et al. Interactions between Th1 cells and Tregs affect regulation of hepatic fibrosis in biliary Atresia through the IFN-gamma/STAT1 pathway. *Cell Death Differ*. 2017;24(6):997–1006.
22. Takei H, Yasuoka H, Yoshimoto K, Takeuchi T. Aryl hydrocarbon receptor signals attenuate lung fibrosis in the bleomycin-induced mouse model for pulmonary fibrosis through increase of regulatory T cells. *Arthritis Res Therapy*. 2020;22(1):20.
23. Xiao K, He W, Guan W, Hou F, Yan P, Xu J, et al. Mesenchymal stem cells reverse EMT process through blocking the activation of NF-kappaB and Hedgehog pathways in LPS-induced acute lung injury. *Cell Death Dis*. 2020;11(10):863.
24. Kitazawa Y, Li XK, Xie L, Zhu P, Kimura H, Takahara S. Bone marrow-derived conventional, but not cloned, mesenchymal stem cells suppress lymphocyte proliferation and prevent graft-versus-host disease in rats. *Cell Transplant*. 2012;21(2–3):581–90.
25. Niu J, Wang Y, Liu B, Yao Y. Mesenchymal stem cells prolong the survival of orthotopic liver transplants by regulating the expression of TGF-beta1. *Turk J Gastroenterol*. 2018;29(5):601–9.
26. Garibaldi BT, D'Alessio FR, Mock JR, Files DC, Chau E, Eto Y, et al. Regulatory T cells reduce acute lung injury fibroproliferation by decreasing fibrocyte recruitment. *Am J Respir Cell Mol Biol*. 2013;48(1):35–43.
27. Kitani A, Fuss I, Nakamura K, Kumaki F, Usui T, Strober W. Transforming growth factor (TGF)-beta1-producing regulatory T cells induce Smad-mediated Interleukin 10 secretion that facilitates coordinated immunoregulatory activity and amelioration of TGF-beta1-mediated fibrosis. *J Exp Med*. 2003;198(8):1179–88.
28. Peng X, Moore MW, Peng H, Sun H, Gan Y, Homer RJ, et al. CD4+CD25+FoxP3+Regulatory Tregs inhibit fibrocyte recruitment and fibrosis via suppression of FGF-9 production in the TGF-beta1 exposed murine lung. *Front Pharmacol*. 2014;5:80.
29. Xie Y, Liu W, Liu S, Wang L, Mu D, Cui Y, et al. The quality evaluation system establishment of mesenchymal stromal cells for cell-based therapy products. *Stem Cell Res Ther*. 2020;11(1):176.
30. Yuan BZ. Establishing a quality control system for stem Cell-Based medicinal products in China. *Tissue Eng Part A*. 2015;21(23–24):2783–90.
31. Daley GQ, Hyun I, Apperley JF, Barker RA, Benvenisty N, Bredenoord AL, et al. Setting global standards for stem cell research and clinical translation: the 2016 ISSCR guidelines. *Stem Cell Rep*. 2016;6(6):787–97.
32. Newman AM, Liu CL, Green MR, Gentles AJ, Feng W, Xu Y, et al. Robust enumeration of cell subsets from tissue expression profiles. *Nat Methods*. 2015;12(5):453–7.
33. Nirmal AJ, Regan T, Shih BB, Hume DA, Sims AH, Freeman TC. Immune cell gene signatures for profiling the microenvironment of solid tumors. *Cancer Immunol Res*. 2018;6(11):1388–400.
34. Shen WC, Lai YC, Li LH, Liao K, Lai HC, Kao SY, et al. Methylation and PTEN activation in dental pulp mesenchymal stem cells promotes osteogenesis and reduces oncogenesis. *Nat Commun*. 2019;10(1):2226.
35. Liu W, Xie Y, Gao T, Huang F, Wang L, Ding L, et al. Reflection and observation: cell-based screening failing to detect HBV in HUMSCs derived from HBV-infected mothers underscores the importance of more stringent donor eligibility to reduce risk of transmission of infectious diseases for stem cell-based medical products. *Stem Cell Res Ther*. 2018;9(1):177.
36. Marinello W, Feng L, Allen TK. Progestins inhibit Interleukin-1beta-Induced matrix metalloproteinase 1 and Interleukin 8 expression via the glucocorticoid receptor in primary human Amnion mesenchymal cells. *Front Physiol*. 2020;11:900.
37. Menon R, Radnaa E, Behnia F, Urrabaz-Garza R. Isolation and characterization human chorion membrane trophoblast and mesenchymal cells. *Placenta*. 2020;101:139–46.
38. Kamali Simsek N, Benian A, Sevgin K, Ergun Y, Goksever Celik H, Karahuseyinoglu S, et al. MicroRNA analysis of human decidua mesenchymal stromal cells from preeclampsia patients. *Placenta*. 2021;115:12–9.
39. Gao Y, Chi Y, Chen Y, Wang W, Li H, Zheng W, et al. Multi-omics analysis of human mesenchymal stem cells shows cell aging that alters Immunomodulatory activity through the downregulation of PD-L1. *Nat Commun*. 2023;14(1):4373.
40. Wu T, Hu E, Xu S, Chen M, Guo P, Dai Z, et al. ClusterProfiler 4.0: A universal enrichment tool for interpreting omics data. *Innov (Camb)*. 2021;2(3):100141.
41. Sakaguchi S. Naturally arising CD4+regulatory t cells for Immunologic self-tolerance and negative control of immune responses. *Annu Rev Immunol*. 2004;22:531–62.
42. Miyara M, Yoshioka Y, Kitoh A, Shima T, Wing K, Niwa A, et al. Functional delineation and differentiation dynamics of human CD4+T cells expressing the FoxP3 transcription factor. *Immunity*. 2009;30(6):899–911.
43. Wang M, Zhao N, Wang C, Jin ZB, Zhang L. Immunomodulatory properties of mesenchymal stem cells: A potential therapeutic strategy for allergic rhinitis. *Allergy*. 2023;78(6):1425–40.
44. Xiao X, Kroemer A, Gao W, Ishii N, Demirci G, Li XC. OX40/OX40L costimulation affects induction of Foxp3+regulatory T cells in part by expanding memory T cells in vivo. *J Immunol*. 2008;181(5):3193–201.
45. Marquez-Curtis LA, Elliott JAW. Mesenchymal stromal cells derived from various tissues: biological, clinical and cryopreservation aspects: update from 2015 review. *Cryobiology*. 2024;104856.
46. Gad ES, Salama AAA, El-Shafie MF, Arafa HMM, Abdelsalam RM, Khattab M. The Anti-fibrotic and Anti-inflammatory potential of bone Marrow-Derived mesenchymal stem cells and nintedanib in Bleomycin-Induced lung fibrosis in rats. *Inflammation*. 2020;43(1):123–34.
47. Takao S, Nakashima T, Masuda T, Namba M, Sakamoto S, Yamaguchi K, et al. Human bone marrow-derived mesenchymal stromal cells cultured in serum-free media demonstrate enhanced antifibrotic abilities via prolonged survival and robust regulatory T cell induction in murine bleomycin-induced pulmonary fibrosis. *Stem Cell Res Ther*. 2021;12(1):506.
48. Hou X, Yin S, Ren R, Liu S, Yong L, Liu Y, et al. Myeloid-Cell-Specific IL-6 signaling promotes MicroRNA-223-Enriched exosome production to attenuate NAFLD-Associated fibrosis. *Hepatology*. 2021;74(1):116–32.
49. Chen Y, Huang Y, Huang R, Chen Z, Wang X, Chen F, et al. Interleukin-10 gene intervention ameliorates liver fibrosis by enhancing the immune function of natural killer cells in liver tissue. *Int Immunopharmacol*. 2024;127:111341.
50. Linton PJ, Bautista B, Biederman E, Bradley ES, Harbertson J, Kondrack RM, et al. Costimulation via OX40L expressed by B cells is sufficient to determine the extent of primary CD4 cell expansion and Th2 cytokine secretion in vivo. *J Exp Med*. 2003;197(7):875–83.
51. Jenkins SJ, Perona-Wright G, Worsley AG, Ishii N, MacDonald AS. Dendritic cell expression of OX40 ligand acts as a costimulatory, not polarizing, signal for optimal Th2 priming and memory induction in vivo. *J Immunol*. 2007;179(6):3515–23.
52. Karulf M, Kelly A, Weinberg AD, Gold JA. OX40 ligand regulates inflammation and mortality in the innate immune response to sepsis. *J Immunol*. 2010;185(8):4856–62.
53. Kumar P, Lele SS, Raghothaman VK, Raghunathan D, Epstein AL, Chiba S, et al. OX40L-JAG1-Induced expansion of Lineage-Stable regulatory T cells involves noncanonical NF-kappaB signaling. *J Immunol*. 2019;203(12):3225–36.
54. Piconese S, Valzasina B, Colombo MP. OX40 triggering blocks suppression by regulatory T cells and facilitates tumor rejection. *J Exp Med*. 2008;205(4):825–39.
55. Caplan AL, Dennis JE. Mesenchymal stem cells as trophic mediators. *J Cell Biochem*. 2006;98(5):1076–84.

## Publisher's note

Springer Nature remains neutral with regard to jurisdictional claims in published maps and institutional affiliations.